JACS
JOURNAL OF THE AMERICAN CHEMICAL SOCIETY
pubs.acs.org/JACS
Article

# Fabrication of Multifunctional Electronic Textiles Using Oxidative Restructuring of Copper into a Cu-Based Metal−Organic Framework

Aileen M. Eagleton, Michael Ko, Robert M. Stolz, Nataliia Vereshchuk, Zheng Meng, Lukasz Mendecki, Adelaide M. Levenson, Connie Huang, Katherine C. MacVeagh, Akbar Mahdavi-Shakib, John J. Mahle, Gregory W. Peterson, Brian G. Frederick, and Katherine A. Mirica*

Cite This: J. Am. Chem. Soc. 2022, 144, 23297−23312



**ABSTRACT:** This paper describes a novel synthetic approach for the conversion of zero-valent copper metal into a conductive two-dimensional layered metal−organic framework (MOF) based on 2,3,6,7,10,11-hexahydroxytriphenylene (HHTP) to form $Cu_3(HHTP)_2$. This process enables patterning of $Cu_3(HHTP)_2$ onto a variety of flexible and porous woven (cotton, silk, nylon, nylon/cotton blend, and polyester) and non-woven (weighing paper and filter paper) substrates with microscale spatial resolution. The method produces conductive textiles with sheet resistances of 0.1−10.1 MΩ/cm$^2$, depending on the substrate, and uniform conformal coatings of MOFs on textile swatches with strong interfacial contact capable of withstanding chemical and physical stresses, such as detergent washes and abrasion. These conductive textiles enable simultaneous detection and detoxification of nitric oxide and hydrogen sulfide, achieving part per million limits of detection in dry and humid conditions. The $Cu_3(HHTP)_2$ MOF also demonstrated filtration capabilities of $H_2S$, with uptake capacity up to 4.6 mol/kg$_{MOF}$. X-ray photoelectron spectroscopy and diffuse reflectance infrared spectroscopy show that the detection of NO and $H_2S$ with $Cu_3(HHTP)_2$ is accompanied by the transformation of these species to less toxic forms, such as nitrite and/or nitrate and copper sulfide and $S_x$ species, respectively. These results pave the way for using conductive MOFs to construct extremely robust electronic textiles with multifunctional performance characteristics.

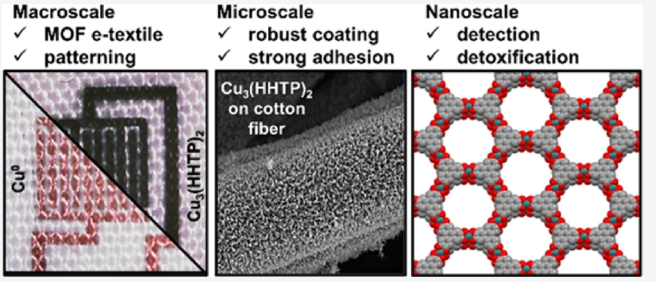


## INTRODUCTION

Multifunctional electronic textiles that sense and adapt to environmental stimuli hold promise for enhancing healthcare,[1−4] protecting against environmental pollution[5,6] and safeguarding from exposure to toxic chemicals and threat agents.[7,8] The recent drive to advance the "Moore's Law of fibers" posits that progress in textile electronics necessitates increasing the functional utility of fabrics at the fiber level.[9−11] While recent innovations have produced textiles capable of physical and chemical detection or detoxification,[12−15] with few exceptions,[8,16−18] these functions typically remain disparate, with limited multifunctional performance that includes real-time assessment of the chemical environment accompanied by a tunable response (e.g., filtration, detoxification, or therapeutic delivery) to the chemical threat.[19−24] Despite these advances, three key challenges currently limit the functional performance of textile-integrated chemically responsive materials. First, chemically reactive interfaces are often insufficiently stable once they are integrated onto textiles.[25−27] Second, textile-integrated chemical sensing materials are typically sensitive to and have difficulty withstanding physical changes, such as heat, abrasion, and detergent-based laundering.[28] Third, there is a general dearth of materials capable of sensitive chemical detection with a broad dynamic range and simultaneous adaptive function applicable to personal protection, environmental application, or healthcare.[29,30] Overcoming these challenges requires conceptual advances and technological approaches that merge the development of exceedingly stable multifunctional sensing materials—capable of maintaining their performance in wearable devices—with robust device integration strategies.[12]

We reasoned that combining water-stable two-dimensional (2D) metal−organic framework (MOF) materials with a proven capacity for multifaceted function in the context of chemical detection,[12,31−34] filtration,[12] electronic transduction,[35,36] energy conversion,[37−39] and storage[40] with an exceptionally robust and scalable methodology for textile integration can pave the way toward mechanically robust

Received: May 24, 2022
Published: December 13, 2022





https://doi.org/10.1021/jacs.2c05510
J. Am. Chem. Soc. 2022, 144, 23297−23312

multifunctional conductive textiles with adaptive function.[12,35,41,42] We and others have employed templated self-assembly to install MOFs on textile substrates such as cellulose,[12,13,43−49] polyester,[12,42,50,51] linen,[13] polyacrylonitrile,[21] silk,[47,52] polypropylene,[16,53,54] and nylon.[55] Despite the rich progress in general methodology for MOF−textile integration, the development of MOF-based electronic textiles has remained extremely limited. While the current examples of conductive MOF e-textiles have demonstrated their potential in chemical sensing,[12,21] energy storage,[42,43] and filtration,[12,21] at least three major limitations currently hinder their applicability. First, the reliance on the in situ growth method has been found to be applicable only to a limited set of substrates (cellulose, polyester, and polyacrylonitrile).[12,21,42,43] This limitation may pose a challenge to broad applicability of this method on a variety of substrates. Second, the demonstrations of MOF-based electronic textiles are currently limited to only two conductive MOFs: $Ni_3$(2,3,6,7,10,11-hexahydroxytriphenylene)$_2$ and $Ni_3$(2,3,6,7,10,11-hexaiminotriphenylene)$_2$ ($Ni_3$(HHTP)$_2$ and $Ni_3$(HITP)$_2$).[12,21,42,43] This limitation in composition of conductive MOF materials severely restricts the functional utility of MOF-based e-textiles. Third, current processes for generating conductive MOF-based textiles lack simplicity, scalability, efficiency, and atom economy. All of the existing methods require heating for in situ growth and suffer from inefficient surface attachment, and some methods require chemical pretreatment of the fabrics for promoting MOF adhesion, thus limiting the scalability and efficiency of the synthetic process.[12,21,42,43] Developing a novel strategy with features of efficiency and scalability that allows for the integration of a diverse set of conductive MOFs onto a variety of textile surfaces with strategic control over their patterning on a broad range of substrates has the potential to advance the "Moore's law of fibers" through the development of MOFs as active components in smart fabric sensors, wearable electronics, and personal protective equipment.

This paper describes a new synthetic method—termed oxidative restructuring—that offers at least five unique attributes for the integration of conductive framework materials into textiles (Figure 1). First, this method demonstrates a new chemical process to install and pattern $Cu_3$(2,3,6,7,10,11-hexahydroxytriphenylene)$_2$ $Cu_3$(HHTP)$_2$ MOF on textile substrates using patterns of $Cu^0$ as a starting material. Restructuring pre-patterned regions of copper metal into MOF generates multifunctional electronic textiles with control over patterns on areas of square centimeters with $\mu$m-scale resolution. Second, the method is extremely versatile in substrate scope. This method leads to conductive coatings of MOFs with sheet resistances of 0.1−10.1 MΩ/cm$^2$ on cotton, paper, nylon, polyester, silk, and nylon/cotton blend over areas exceeding 100 cm$^2$ with control over the pattern, morphology, and orientation of MOFs on these substrates. Third, the MOF/textile composites generated using this approach are extremely robust and are capable of withstanding a variety of physical (abrasion, heat, and laundering) and chemical washes with detergent and bleach, while maintaining their chemical sensing performance. Fourth, oxidative restructuring proceeds under mild aqueous conditions that are consistent with several requirements for green chemical processes. Fifth, this method is rapid. The rate of oxidative restructuring can be tuned by adjusting the oxidant, with transformation reaching completion within 15 min (in the presence of $H_2O_2$ oxidant) or within 12 h under ambient conditions. The chemical transformation in the presence of the $H_2O_2$ is the most rapid technique for MOF formation reported to date.[12−15,45,46] Taken together, these unique attributes of oxidative restructuring enable rapid, efficient, and scalable fabrication of extremely robust electronic textiles that detect NO and $H_2S$ with experimentally determined detection limits of 1 ppm, while additionally demonstrating the capability for decontaminating these gases into less toxic products ($NO_2^-$ or $NO_3^-$ and $S^0$ or copper sulfide, respectively). The oxidative restructuring method enables the development of multifunctional devices with synergistic effects, afforded by the strategic combination of MOFs and textiles, and has the potential to advance wearable electronic applications by harnessing the capability for simultaneous chemical detection and detoxification.

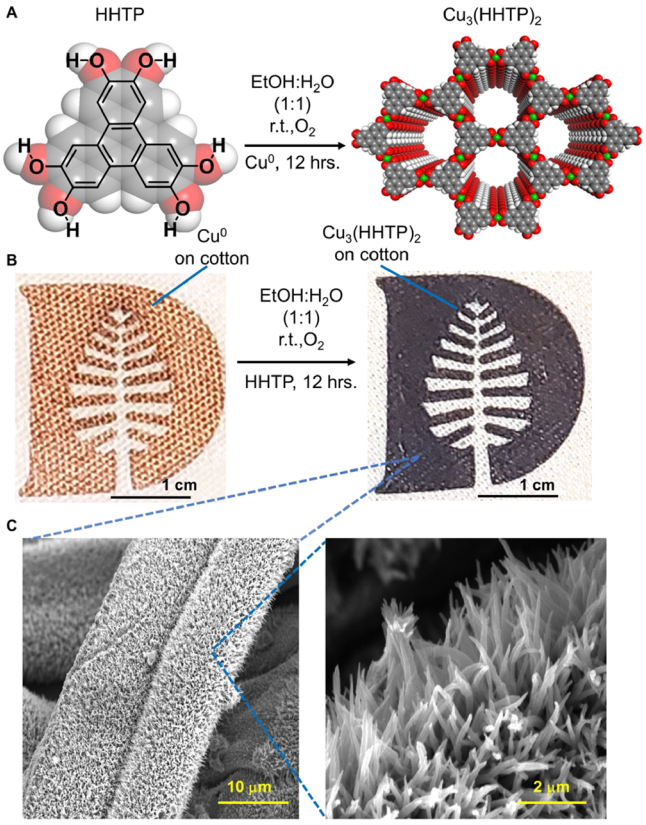


**Figure 1.** (A) Synthetic scheme for the formation of $Cu_3$(HHTP)$_2$ MOF using oxidative restructuring. (B) Conversion of patterned $Cu^0$ on cotton into patterns of textile-integrated MOF. The Dartmouth logo is reproduced with permission from the university. (C) Scanning electron micrographs showing $Cu_3$(HHTP)$_2$ MOF on cotton at 10,000× and 60,000× magnification.

## RESULTS AND DISCUSSION

**Oxidative Restructuring of $Cu^0$ into $Cu_3$(HHTP)$_2$.** In traditional solvothermal synthesis of $Cu_3$(HHTP)$_2$ MOF, the metal salt, organic ligand, solvent, temperature, and oxidant are all important factors in achieving the formation of the framework material.[41,56,57] Compared to the solvothermal method, oxidative restructuring has two important distinctions: (i) the source of metallic nodes comes from a zero-valent metal pre-patterned on a porous substrate and (ii) this method forms MOF at room temperature with the oxidant influencing the rate of MOF formation (within 12 h with $O_2$ as the oxidant or within 15 min using $H_2O_2$ as the oxidant) (Figure 1A).


https://doi.org/10.1021/jacs.2c05510
J. Am. Chem. Soc. 2022, 144, 23297−23312

Oxidative restructuring capitalizes on the ability to deposit and pattern zero-valent metallic features on substrates and convert these features into MOFs in the presence of the appropriately chosen organic linkers and oxidants. The metal-coated substrate, when added to a solution containing an oxidizing agent and ligand, can generate metal cations that can coordinate to the deprotonated organic ligands. While restructuring $Cu^0$ to form three-dimensional MOFs has been previously applied to generate Cu-BTC MOFs (BTC = benzene-1,3,5-tricarboxylic acid) on solid copper clad plates,[58] copper wires,[59] glass,[60] and polyethylene terephthalate surfaces,[61] this strategy has remained entirely unexplored for 2D conductive MOFs and has not been previously adapted to textiles. Although Bradshaw and coworkers demonstrated the first example of anodic electrosynthesis of $Cu_3(HHTP)_2$ from electrodeposited Cu on conductive substrates (fluorine tin oxide and $Au/SiO_2$ glass),[62] this electrosynthetic strategy is not extendable to non-conductive substrates. Inspired by the initial feasibility of restructuring $Cu^0$ features on solid substrates into Cu-containing MOFs, this study expands this concept for the first time to the integration of the conductive $Cu_3(HHTP)_2$ MOF on a variety of textile substrates. The mild and rapid approach described herein is capable of producing extremely robust patterned multifunctional electronic textiles on diverse substrates for simultaneous detection, filtration, and detoxification of toxic reactive gases.

**Conversion of $Cu^0$ Particles into MOFs.** In our initial studies, we employed $Cu^0$ nanoparticles ($d$ = 25 nm) and microparticles ($d$ = 45 $\mu$m) to demonstrate the feasibility of conversion of zero-valent Cu into $Cu_3(HHTP)_2$ MOF (Figures S1 and S2). While the $Cu^0$ microparticles in the presence of oxidant ($O_2$ or $H_2O_2$) in $H_2O$:EtOH (1:1 volume) solution containing HHTP reacted to produce $Cu_3(HHTP)_2$ MOF, they also contained residual $Cu^0$, as evidenced by the $Cu^0$ diffraction peak in powder X-ray diffraction (PXRD) located at 43 and 50° 2$\theta$ (Figure S1). In contrast, the use of $Cu^0$ nanoparticles under indistinguishable conditions led to their complete conversion to $Cu_3(HHTP)_2$ MOF, as evidenced by the lack of detectable $Cu^0$ diffraction peaks by PXRD. The size of the $Cu^0$ particles not only influenced the extent of conversion of $Cu^0$ into MOF, but also the overall morphology of the MOF crystallites. Scanning electron microscopy (SEM) showed that $Cu^0$ microparticles led to irregular crystallite formation, whereas the $Cu^0$ nanoparticles yielded uniform and regular rod-like morphology of the MOF (Figure S2). We attributed the complete conversion of the copper nanoparticles to $Cu_3(HHTP)_2$ to the higher surface to volume ratio of the smaller nanoparticles when compared to the microparticles. The initial formation of MOF crystallites on the Cu microparticle surface could have precluded access of the solvent and dissolved ligand to the metal source due to the larger particle size, inhibiting further MOF formation.[60] After confirming the feasibility of forming layered 2D MOF through the conversion of $Cu^0$ nanoparticles using oxidative restructuring, we proceeded to expand this concept by restructuring patterns of $Cu^0$ films having nanoscale thickness, pre-deposited on porous and flexible substrates into MOF coatings.

**Integration of $Cu_3(HHTP)_2$ MOF onto Cotton Using Oxidative Restructuring.** To achieve the growth of $Cu_3(HHTP)_2$ on porous and flexible substrates using oxidative restructuring, we first thermally evaporated a thin layer of Cu metal (120 nm) onto the cotton surface (4.0 cm × 2.5 cm) to form a template for MOF synthesis (Figure 1B). Subsequent placement of the Cu-coated cotton into a solution of 10 mg of HHTP dissolved in 10 mL of $H_2O$:EtOH (1:1 volume) open to ambient air for 12 h led to the formation of MOF directly on the cotton [5−7% $Cu_3(HHTP)_2$ mass loading for 0.75 $cm^2$ and 0.49 ± 0.1 mg of $Cu_3(HHTP)_2/cm^2$] (Figure 1B and Table S1). SEM analysis demonstrated conformal coating of cotton fibers by radially oriented MOF crystallites (Figures 1C and S3) and uniform coating on the microscale (Figure S4).

**Characterization of Restructuring $Cu^0$ into MOF on Cotton.** PXRD analysis showed complete conversion of $Cu^0$ to $Cu_3(HHTP)_2$ within 12 h, as evidenced by the disappearance of the Cu (111) and Cu (200) planes located at 43 and 50° 2$\theta$ and increasing intensity of the (100) plane of $Cu_3(HHTP)_2$ at 4.7° 2$\theta$ (Figure 2).[41,56,63] Before the 12 h time mark, PXRD showed the presence of residual $Cu^0$ (Figure S5). No copper oxide intermediate was observed by PXRD.

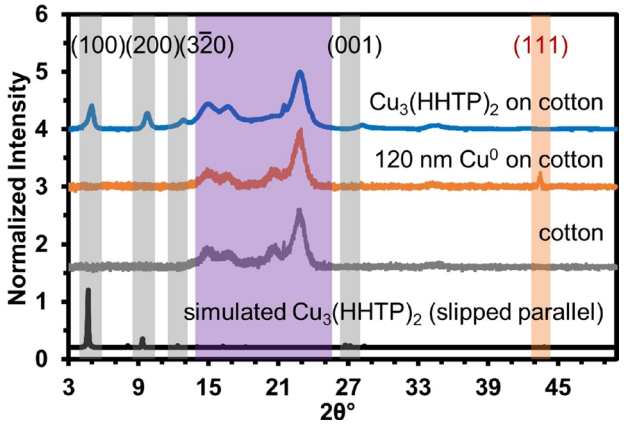


**Figure 2.** Characterization of $Cu_3(HHTP)_2$ on cotton using PXRD. Gray shading denotes MOF diffraction peaks, purple shading represents cotton diffraction peaks, and orange shading shows the $Cu^0$ diffraction peak at 43° 2$\theta$. The simulated powder pattern of $Cu_3(HHTP)_2$ calculated using Materials Studio is presented for comparison. The structure of the simulated MOF has been optimized for the geometry and lowest energy state.

Bubbling pure $O_2$ resulted in the onset of MOF conversion at 5 min (Figure S6). Hydrogen peroxide ($H_2O_2$) also worked to increase the rate of MOF formation, which was confirmed by PXRD analysis to be complete within 15 min (Figure S7). However, the use of $H_2O_2$ as an oxidant diminished the morphological uniformity of the MOF on textile (Figure S8). All oxidant conditions examined produced conductive MOF coatings on textiles with sheet resistances in the range of 2.4−6.0 MΩ/$cm^2$; see Section S2.2. for more details (Tables S2−S4). The resistance of $Cu_3(HHTP)_2$ on cotton, obtained under ambient conditions, $O_2$ bubbling, or addition of $H_2O_2$, was measured using a two-point probe method at time points throughout the formation process (Tables S2−S4 and Section S4.6). The resistance measurements for the formation of $Cu_3(HHTP)_2$ on cotton after the reaction period under ambient conditions, bubbling $O_2$, and $H_2O_2$ were all in the low MΩ/$cm^2$ range (Tables S2−S4).

Surface analysis of MOF on cotton using X-ray photoelectron spectroscopy (XPS) confirmed the elemental composition of $Cu_3(HHTP)_2$, matching reported literature with the elements O, C, and Cu; XPS also confirmed mixed valency of Cu ($Cu^{2+}$ = 68.6%, $Cu^+$ = 31.4%) within the framework (Figure S9).[64] The surface area of $Cu_3(HHTP)_2$


https://doi.org/10.1021/jacs.2c05510
J. Am. Chem. Soc. 2022, 144, 23297−23312

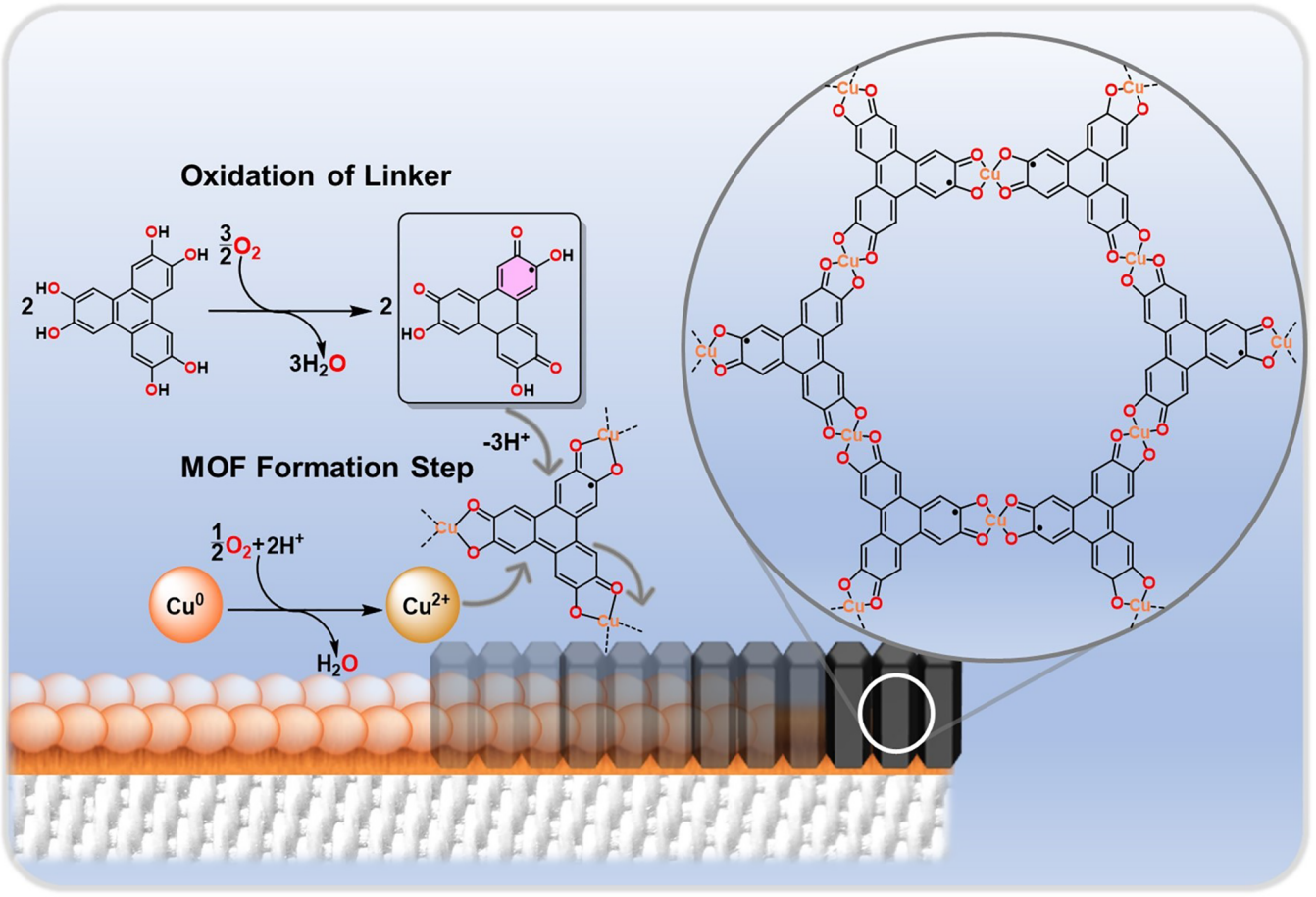


**Figure 3.** Proposed mechanism of oxidative restructuring of $Cu^0$ metal into $Cu_3(HHTP)_2$ MOF. The presence of oxygen promotes the oxidation of copper metal, while the HHTP linker is transformed from a tris-catechol to a tris-semiquinone monoradical.

MOF coated on cotton and $Cu_3(HHTP)_2$ restructured from $Cu^0$ nanoparticles ($d$ = 25 nm) was measured using $N_2$ gas adsorption isotherms and calculated using Brunauer–Emmett–Teller (BET) theory. The isotherm for the $Cu_3(HHTP)_2$ on cotton was a type IV adsorption–desorption curve, indicating that the MOF cotton composite is a mesoporous material and the calculated surface area for the composite was 9.03 ± 0.02 $m^2/g$[65−67] and has an enhanced surface area over bare cotton (Figure S10A).[12] The calculated surface area from the BET analysis of $Cu_3(HHTP)_2$ restructured from $Cu^0$ nanoparticles (Section S4.8.) was 191.65 ± 0.01 $m^2/g$ (Figure S10B), which is in congruence with the calculated surface area of $Cu_3(HHTP)_2$ formed from the standard solvothermal synthesis.[68]

Thermogravimetric analysis of $Cu_3(HHTP)_2$ on cotton displayed one distinct mass loss step (Figure S11). The mass loss step with an onset temperature of ∼319 °C with a mass change of 4.3 mg was attributed to the thermal decomposition of the $Cu_3(HHTP)_2$ framework and cotton (Figure S11).[62] Cotton and $Cu_3(HHTP)_2$ bulk powder both showed one major mass loss step with onset temperatures of 330 and 258 °C, respectively (Figure S11). $Cu_3(HHTP)_2$ in composite with the cotton has an onset temperature that is between cotton and bulk MOF and a large change in mass that is comparable to cotton.

**Substrate Scope.** The versatility of oxidative restructuring lies in the ability to deposit the metal precursor onto a variety of substrates. To demonstrate the general applicability of the method, we thermally evaporated $Cu^0$ (thickness = 120 nm) and investigated its restructuring into MOF on seven substrates with different chemical compositions and surface chemistries ranging from natural to synthetic polymers and woven (cotton, silk, nylon, nylon/cotton blend, and polyester) to non-woven (weighing paper and filter paper) fiber structures (Figure S12). Reaction conditions (Section S2.2) were kept constant for all substrates. The lateral features of Cu patterns with mm- to cm-scale dimensions generated by thermal evaporation were effectively converted to $Cu_3(HHTP)_2$ MOF to generate patterns with dimensions indistinguishable from the initially patterned Cu at the sub-mm scale (Figure S12). The oxidative restructuring method was also tested on glass, mica, and polymethyl methacrylate (PMMA) plastic. While the chemical transformation was successful, the MOF did not adhere strongly to the glass, mica, or PMMA. This test demonstrated that the MOF adhesion on porous substrates was more robust than on non-porous surfaces (Figure S12). We attribute the robust adhesion of $Cu_3(HHTP)_2$ MOF to porous polymeric substrates to the combination of mechanical interlocking of MOF crystallites on fibrous substrates and to the molecular level adhesion that can be promoted by the copper–polymer interphase that can form during thermal evaporation of metal on polymeric surfaces.[69]

SEM analysis after deposition of the $Cu^0$ layer on various textile substrates showed a smooth coating of copper film that subsequently converted into $Cu_3(HHTP)_2$ MOF (Figure S13). The MOF exhibited nanowire morphology on all substrates


https://doi.org/10.1021/jacs.2c05510
J. Am. Chem. Soc. 2022, 144, 23297−23312

examined. The sheet resistance readings for MOF patterned on cotton ranged from 1.0 to 10.1 MΩ/cm$^2$ across 1.5 cm on swatches (1.5 cm × 0.5 cm) ($n$ = 31). All woven textiles with a layer of 120 nm of Cu$^0$ were not conductive on the macroscopic scale ($R$ > 50 MΩ over 0.75 cm) due to the discontinuity of the Cu$^0$ coating evaporated on a woven substrate, whereas smooth and non-woven Cu-coated surfaces, such as weigh paper and filter paper, showed low resistances (<100 Ω over 0.75 cm) (Table S5) commensurate with a continuous film of Cu$^0$.[70] For further analysis of the characterization and performance of MOF-patterned surfaces, we chose cotton—which is ubiquitously used in the textile industry—as a model system to demonstrate the capabilities of oxidative restructuring for integration of MOFs on textiles.[71]

**Controlled Patterning of MOF on Cotton.** Oxidative restructuring allowed for intricate patterns of Cu$^0$ to be restructured into $Cu_3(HHTP)_2$ MOF with microscale fidelity (Figures 1B and S14). $Cu_3(HHTP)_2$ selectively grew only on pre-deposited patterns of Cu$^0$ (Figure S14). We observed no MOF formation on bare cotton regions (Figure S14C) via PXRD. Energy-dispersive X-ray spectroscopy (EDS) mapping supported the precise growth of $Cu_3(HHTP)_2$ within regions of pre-deposited Cu$^0$ (Figure S15). The precise location for Cu$^0$ deposition and conversion to $Cu_3(HHTP)_2$ was confirmed through the spatial mapping of Cu, C, and O emission lines by EDS. To quantify the fidelity of pattern conversion from Cu$^0$ to $Cu_3(HHTP)_2$ MOF, we evaporated a set of Cu$^0$ interdigitated electrodes (IDEs) on cotton and observed the transformation after oxidative restructuring using a digital microscope and EDS mapping (Figures S16 and S17). The average lateral area of the $Cu_3(HHTP)_2$ pattern was ∼0.1 and 0.2 mm$^2$ greater than the average lateral area of the Cu$^0$ IDE for the analyzed optical and EDS mapped image, respectively (Figure S17C and Section S4.15). Thus, while the overall pattern of IDEs was preserved, some blurring of features occurred on the microscale.

**Proposed Mechanism of Oxidative Restructuring of $Cu_3(HHTP)_2$ MOF on Porous Substrates.** Oxidative restructuring is conceptually analogous to electrochemical reactions that restructure Cu$^0$ metal to Cu oxides and other Cu species.[72] The proposed mechanism, detailed in Figure 3, features three key steps: (1) the transformation of zero-valent copper to divalent copper; (2) the reduction of $O_2$ to $H_2O_2$ that is coupled to the oxidation of copper; (3) the oxidation of the tri-catechol linker to the tris-semiquinone, followed by the coordination to the divalent copper to form the $Cu_3(HHTP)_2$ MOF.[73−75] Based on this proposed transformation, oxidative restructuring is contingent on at least three key experimental parameters: (1) the thermodynamic favorability of Cu$^0$ corrosion to cationic copper species under aerated ambient conditions at an acidic pH;[76] (2) the reduction potential of oxygen (the oxidizing agent), which is more favorable in acidic conditions;[77] and (3) a high ratio of ligand to metal (∼12:1) because the deprotonation of ligand contributes to the acidity of the solution and maintains a highly effective concentration of ligand near the metal surface to ensure the formation of $Cu_3(HHTP)_2$ on textiles, rather than aggregation and precipitation of MOF crystallites.

$O_2$ plays a critical role in oxidizing Cu$^0$ to Cu$^{2+}$ ($E_r$ = 0.337 V), which is possible in acidic solution,[78] or copper oxide intermediates ($E_r$ = 0.26 V for $Cu_2O$ and $E_r$ = 0.06 V for CuO/$Cu(OH)_2$), which is possible in alkaline conditions.[72] The standard reduction potential of $O_2$ is drastically different in acidic conditions ($E_r$ = 1.229 V, pH = 0) compared to basic conditions ($E_r$ = 0.401 V, pH = 14).[72,78] The crucial function of oxygen in the oxidative restructuring mechanism was confirmed by excluding oxygen from the reaction; air-free conditions led to no observable MOF formation and complete retention of Cu$^0$ on cotton (Figure S18). Expanding this method to restructure thermally evaporated patterns of Ni$^0$ into $Ni_3(HHTP)_2$ under conditions developed in this study were unsuccessful, leading to retention of Ni$^0$ on cotton upon exposure to $O_2$(g) and HHTP (Figure S19). We, therefore, conclude that the conditions presented herein are optimized for $Cu_3(HHTP)_2$ and are not optimized for the formation of $Ni_3(HHTP)_2$, possibly due to the passivation of Ni$^0$ through the formation of a nickel oxide layer that could be inert to MOF formation.[79]

The choice of solvent is critical for promoting the process of oxidative restructuring of Cu metal into MOF. The deprotonation of the HHTP ligand under reaction conditions can contribute to the decrease in the pH range to 5.0−5.7 pH, which can increase the reduction potential of $O_2$.[56] The ability to deprotonate the linker also promotes proton coupled electron transfer (PCET) during the reduction of oxygen (Figure 3). To determine the role of protic and aprotic solvents in promoting the conversion process, we performed oxidative restructuring in different solvents. We corroborated that $Cu_3(HHTP)_2$ on cotton forms favorably in ethanol, water, and $H_2O$:EtOH (1:1 volume) (Figure S20). However, the MOF on cotton did not form in acetone, $H_2O$:acetone (1:1 volume), or DMSO (Figure S20). We attribute this observation to the favorable role of ethanol and water in promoting PCET and encouraging the deprotonation of the HHTP ligand.

In oxidative restructuring, the in situ generated cationic Cu$^+$/Cu$^{2+}$ species can react with the oxidized deprotonated ligand to form $Cu_3(HHTP)_2$ MOF. In a traditional solvothermal system, the metal-to-ligand ratio conditions typically employ a 2:1 ratio to ensure that all of the ligand is consumed by Cu$^{2+}$ to form the $Cu_3(HHTP)_2$ MOF.[41] However, a successful reaction utilizing oxidative restructuring resulting in full coverage of the textile swatch required a metal-to-ligand ratio of 1:12; a higher ratio of metal to linker results in MOF precipitation instead of deposition on the textile.

We considered at least three pathways that can lead to oxidative restructuring: (i) oxidation of copper metal to the cationic Cu species that can then react with the oxidized linker to form MOFs or (ii) formation of MOFs from a copper oxide intermediate, and (iii) the possibility of oxidation of HHTP by dissolved oxygen and its subsequent contribution to the corrosion of Cu. While we did not observe any copper oxide intermediate during our investigation of oxidative restructuring under optimized conditions, we decided to probe the feasibility of restructuring copper oxide and copper hydroxide powder precursors into $Cu_3(HHTP)_2$ (Figure S21). Restructuring of copper hydroxide, $Cu(OH)_2$, resulted in favorable MOF formation (Figure S21A,D), as confirmed by SEM and PXRD (Figure S21E). In contrast, we did not observe MOF formation from $Cu_2O$. This result may be due to poor solubility of $Cu_2O$ and kinetic inhibition of the oxidative restructuring with monovalent copper (Figure S21B,E). While MOF formation did occur from CuO, the transformation into $Cu_3(HHTP)_2$ was incomplete, as evidenced by residual peaks in PXRD corresponding to (111) and (202) of CuO (Figure S21C,E). To corroborate the formation of Cu oxides on cotton


https://doi.org/10.1021/jacs.2c05510
J. Am. Chem. Soc. 2022, 144, 23297−23312

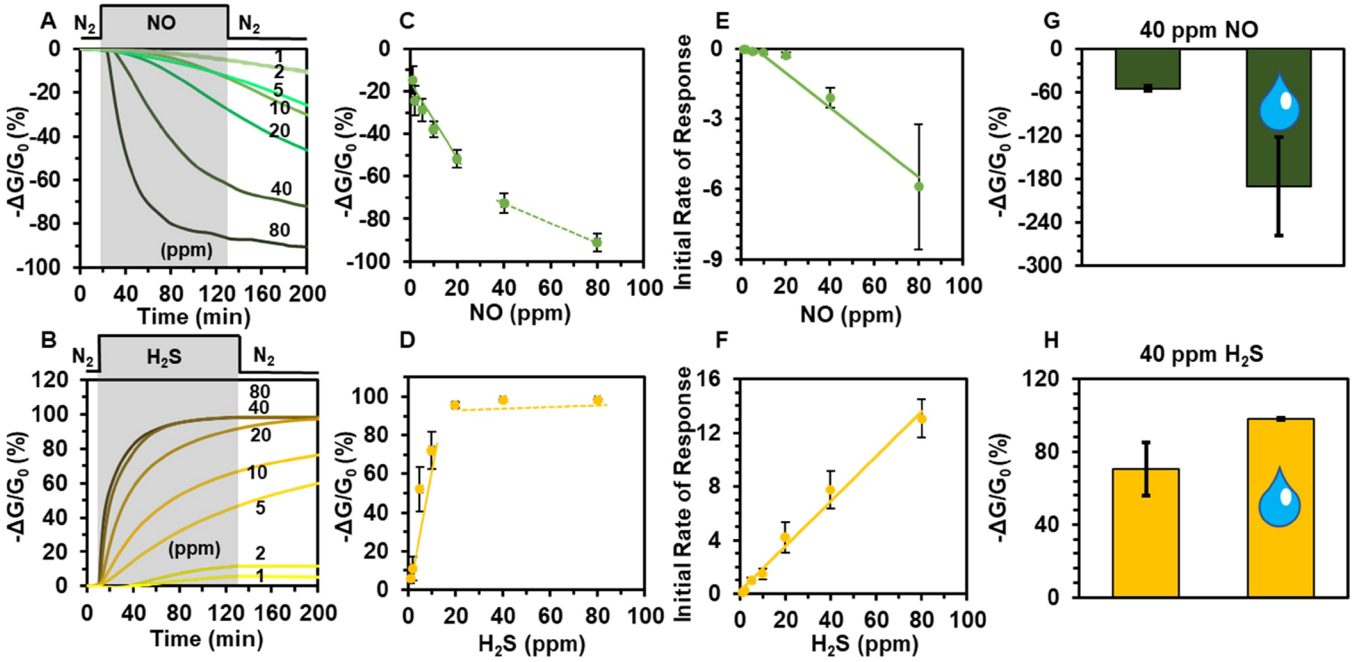


**Figure 4.** Sensing performance of $Cu_3(HHTP)_2$ on cotton devices exposed to gaseous analytes. Representative sensing traces showing the change in conductance $-\Delta G/G_0(\%)$ over time (min) upon exposure of devices to (A) NO and (B) $H_2S$ ranging from 1 to 80 ppm diluted with $N_2$ at room temperature. The gray region represents the duration of exposure to the analyte, and the white region represents baseline and recovery in $N_2$. (C) Concentration dependence plot of sensing response of the $Cu_3(HHTP)_2$ MOF on cotton to NO (1−80 ppm) reveals a linear response from 1 to 40 ppm for NO (solid line $y = -1.75x + 18.16$ $R^2 = 0.98$) with saturation occurring after 40 ppm. (D) Concentration dependence plot of sensing response of the $Cu_3(HHTP)_2$ MOF on cotton to $H_2S$ (1−80 ppm) reveals a linear response from 1 to 20 ppm for $H_2S$ (solid line $y = 7.65x + 0.899$, $R^2 = 0.93$) with saturation occurring after 20 ppm. The initial rates of response $-\Delta G/G_0(\%)/s$, measured in first 2 min of exposure, as a function of concentration toward (E) NO 5−20 ppm ($y = -0.0096x - 0.0693$, $R^2 = 0.99$), NO 20−80 ppm ($y = -0.0941x + 1.638$, $R^2 = 0.99$), and (F) $H_2S$ ($y = 0.17x + 0.19$, $R^2 = 0.99$). (G) Saturation sensor response at 40 ppm of NO in dry nitrogen (solid bar) and in the presence of 5000 ppm water (with water droplet). (H) Saturation sensor response at 40 ppm of $H_2S$ in dry nitrogen (solid bar) and in the presence of 5000 ppm water (with a water droplet).

during oxidative restructuring, a control reaction was conducted with $H_2O$:EtOH (1:1 volume) in the absence of a HHTP linker under ambient conditions. After a 12 h period, there was no evidence of copper oxide formation, based on PXRD and XPS analysis (Figure S22). In summary, while the possibility of a copper oxide intermediate during oxidative restructuring cannot be excluded, this intermediate was not directly detected in the optimized reaction conditions.

To confirm the formation of Cu ions in solution during the oxidative restructuring process, we used inductively coupled plasma mass spectrometry (ICP-MS) to quantify the amount of Cu ions in solution during the course of the reaction (Figure S23). We performed ICP-MS analysis of copper in solution under three conditions: (1) under optimized reaction conditions that included evaporated Cu on cotton, HHTP linker, and $O_2$ gas, (2) in the absence of a HHTP linker, and (3) in the absence of oxygen. Under optimized reaction conditions, ∼130 $\mu$M of copper ions was present in solution, confirming that in situ generated Cu ions play a critical role in the oxidative restructuring process. This concentration of Cu ions accounts for 50% of all Cu species in the reaction vessel, which suggests that the remainder of the copper metal is maintained at a high effective concentration near the surface of the cotton contributing to the templation of the MOF on the surface and retention of the original Cu pattern as it restructures into MOF. The concentration of in situ generated copper ions in the solution remained at ∼110 to 160 $\mu$M for standard reaction conditions and conditions without HHTP, suggesting that the presence of the linker likely does not compete with oxygen to promote extraction of copper metal into solution (Figure S23). The absence of oxygen reduced the concentration of in situ generated Cu ions in solution to 59 $\mu$M on average (Figure S23), such that only 25% of the copper that was originally on the cotton partitioned into solution during the reaction time (12 h). Taken together, these findings confirm that oxygen plays a key role in the transformation of $Cu^0$ into in situ generated cationic copper species during the oxidative restructuring process.

**Device Yields.** Oxidative restructuring is capable of generating electrically conductive swatch-based devices across large surface areas of textiles. This synthetic method afforded high yields of $Cu_3(HHTP)_2$ MOF-coated cotton devices with >96% ($n$ = 50). These devices were considered functional when two-point resistance readings had an average of approximately 2 MΩ across 1.5 cm devices and PXRD showed evidence for MOF growth. $Cu_3(HHTP)_2$ devices with resistances five times greater than the average of 2 MΩ were discarded (around 10 MΩ) in the calculation of the yield. The selected devices were assessed by chemiresistive sensing and detoxification of gases.

**Chemical Detection of Gases.** To demonstrate the synergistic effects of multifunctional 2D MOFs on porous textiles, we measured the performance of these materials in the context of chemiresistive detection. We focused on the detection of two representative gases NO and $H_2S$ that play multifunctional roles as toxic gases[80,81] as well as gasotransmitters.[82,83] While $Cu_3(HHTP)_2$ MOFs in the composite with graphite either in a ball-milled blend[63] or on a shrinkable


https://doi.org/10.1021/jacs.2c05510
J. Am. Chem. Soc. 2022, 144, 23297−23312

polymer film[56] have also been reported by our group for the detection of $H_2S$ and NO, the responses in normalized conductance were approximately 10 times lower than the sensing response reported in this paper for both analytes (Figure 4). This paper provides the first report of a comprehensive investigation of the sensing response to $H_2S$ and NO through spectroscopic analysis of the interactions between $Cu_3(HHTP)_2$ with these analytes.

To achieve chemical detection, conductive textile swatches coated with the $Cu_3(HHTP)_2$ MOF (1.5 cm × 0.5 cm) were placed into an airtight custom Teflon enclosure equipped with gold-coated pins that formed electrical contacts to the flexible devices (Figure S24). Sensing was performed under a constant applied potential of 1.0 V across each device and through the measurement of the resulting current with a potentiostat in chronoamperometric mode. We delivered controlled doses of desired analytes to the enclosure using mass flow controllers by diluting the gaseous analytes ($H_2S$ and NO) with $N_2$. Each gas at a specific concentration (80 ppm, 40 ppm, 20 ppm, 10 ppm, 5 ppm, 2 ppm, or 1 ppm) was delivered for 2 hours, followed by a recovery period of 2 hours with a $N_2$ stream. The devices with $Cu_3(HHTP)_2$ MOF exhibited a concentration-dependent response to $H_2S$ and NO, as illustrated in Figure 4, with the normalized response ($-\Delta G/G_0$).

**Quantitative Assessment of Chemical Detection.** NO and $H_2S$ delivered at a concentration of 80 ppm exhibited dosimetric responses of −87 and 98% $-\Delta G/G_0$, respectively (Figures 4A,B and S25). The dosimetric response revealed that the interaction of $Cu_3(HHTP)_2$ with NO irreversibly decreased the resistance of the devices, whereas exposure to $H_2S$ irreversibly increased the resistance of the devices. The directionality of response to NO and $H_2S$ at 80 ppm was consistent with previous studies of $Cu_3(HHTP)_2$ by our group,[63] but showed an increase by 2 orders of magnitude, potentially arising from favorable dispersion of $Cu_3(HHTP)_2$ on cotton. Concentration-dependent studies of analytes between 1 and 80 ppm showed linearity of $-\Delta G/G_0$ response at 1−20 ppm NO and 1−10 ppm $H_2S$ after ∼110 min exposure, with higher concentrations leading to saturation of devices (Figures 4C,D and S25). The overall percent response of the devices to $H_2S$ and NO gave an experimentally determined limit of detection of 1 ppm (Figure S25). Compared to $Ni_3(HHTP)_2$ on cotton, the only other reported MOF-based textile device for chemiresistive detection of $H_2S$ and NO, the overall % response was similar for both gases.[12]

While reaching the saturation point in a chemiresistive device may be time-consuming, the analysis of the initial rates of response (initial rate of response within 2 min) can offer a rapid method of analysis.[84−86] Figure 4E,F shows the initial rates of response ($-\Delta G/G_0$/s) of $Cu_3(HHTP)_2$ fabric devices upon 2 min exposure to $H_2S$ and NO. This approach provides a rapid strategy for concentration-dependent detection of gases. The plot in Figure 4E shows two distinct linear regions from 5−20 to 20−80 ppm, indicating two different processes; at lower concentrations, there is a low rate indicating an induction period in which an autocatalytic process is taking place. The slope of the linear regression line in Figure 4F represents the rates of response in the concentration range of 1−80 ppm $H_2S$, showing a linear correlation with concentration. The analysis of initial rates of response in the detection of $H_2S$ occurs more rapidly compared to NO; the slope $(-(\Delta G/G_0)/[\text{analyte}]\Delta t)$ in Figure 4F is an order of magnitude higher than the rate of response to NO (Figure 4E). This observation indicated that the initial rate of response was dependent on the type of interaction of the analyte with the MOF (vide infra). The rate constants for chemiresistive gas sensing of NO and $H_2S$ were determined to be $7.82 \times 10^{-5}$ and $1.25 \times 10^{-4}$ $s^{-1}$, respectively (Figure S26). Studies of user-to-user reproducibility showed that the saturation of two different $Cu_3(HHTP)_2$ on cotton devices with 40 ppm $H_2S$ between two different users was indistinguishable (Figure S27). $Cu^0$ on weigh paper did not respond to 80 ppm NO and $H_2S$ in $N_2$, whereas $Cu_3(HHTP)_2$ on weigh paper did respond; this result confirmed that the $Cu_3(HHTP)_2$ MOF has an enhanced sensing response over $Cu^0$ (Figure S28).

**Chemiresistive Sensing of Gases in Humid Conditions and in Air.** Encouraged by the sensing responses to NO and $H_2S$ in $N_2$, we evaluated the ability of the devices to detect NO and $H_2S$ in a humid environment (18% relative humidity, 5000 ppm $H_2O$) (Figure S29). The detection of NO in 18% relative humidity surpassed the detection of this analyte in dry conditions: an increase of response by 136% for 40 ppm (Figure 4G) and by 92% for 80 ppm. (Figure S30A). We attributed the increase in response to NO and $H_2S$ in humid conditions to the stabilizing effects of Brønsted acid site interactions upon adsorption of these target analytes.[87,88] BET analysis of $Cu_3(HHTP)_2$ MOF bulk powder confirmed its excellent capacity for water uptake (0.35 g $H_2O$/g MOF) and a high specific surface area for water adsorption (881.31 ± 55.6 $m^2$/g) (Figure S30C). These results for water uptake were comparable to a water harvesting COF material reported by Yaghi and coworkers.[89] To simulate NO detection in the presence of oxygen, we tested the sensing performance of $Cu_3(HHTP)_2$ on cotton to $NO_2$ in air at 40 ppm. The sensing performance of $NO_2$ at 40 ppm in air was 38% lower than the sensing performance of NO in $N_2$ conditions (Figure S31).

The detection of $H_2S$ at 40 and 80 ppm in humid conditions (18% relative humidity, 5000 ppm $H_2O$) had a ∼30 to 40% increase in sensing performance when compared to sensing in a $N_2$ environment (Figures 4H and S30B). Taken together, these results indicate that $Cu_3(HHTP)_2$ on cotton exhibits excellent stability and retains its sensing performance in realistic environments (in the presence of humidity and air). However, the differences between the sensing response in $N_2$ and under ambient conditions suggest that chemiresistive devices made from this MOF will likely require appropriate calibration in the testing environment.

**Stability and Regenerability of Chemiresistive $Cu_3(HHTP)_2$ on Cotton Devices.** Retaining the function of chemical sensing is important for robust and re-usable wearable e-textiles. Maintaining full functionality in wearable devices after severe stresses such as extended wear, rigorous use, and washing of textiles is crucial for practical applicability. However, these performance features often remain difficult to achieve in wearable materials due to poor interfacial contact between the material and the textile or the inherent stability of the material. Thus, developing and testing materials that can retain full functionality such as sensing and detoxification is critical. Since the chemiresistive devices saturated their response after the exposure to $H_2S$ and NO, we investigated conditions to restore the sensing function after previous exposure. We first assessed the regenerability of the $Cu_3(HHTP)_2$ on cotton by running a stream of dry nitrogen over the devices or washing the devices with water. After exposure to $H_2S$ or NO at 80 ppm, the devices exhibited full saturation and limited recovery under a continuous stream of


https://doi.org/10.1021/jacs.2c05510
J. Am. Chem. Soc. 2022, 144, 23297−23312

nitrogen. A washing step in water restored the normalized sensing response of the devices to NO and $H_2S$, within error compared to the fresh devices (Figure S32). This recovery of the devices upon washing with water was comparable to the previous observation by our group for textile sensors employing $Ni_3(HHTP)_2$ and $Ni_3(HITP)_2$ for the detection of $H_2S$ and NO.[12] The recoverability after washing $H_2S$ saturated MOF on cotton devices in water could be occurring because hydrogen sulfide and reduced sulfur species can undergo ionization in water to form soluble bisulfide or polysulfide anions.[90] ICP-MS analysis confirmed that sulfide species washed off of $Cu_3(HHTP)_2$ on cotton exposed to $H_2S$ (Table S7). A possible explanation for the recovery of the MOF on cotton after NO exposure is the possibility of adsorbed NO or $NO_x$ species reacting with oxygen in water to form nitrite or nitrate species, which would promote desorption.[91] Colorimetric test strips revealed nitrate, in the concentration range of 10−25 ppm, washed off of NO-exposed $Cu_3(HHTP)_2$ on cotton in water (Figure S33).

After establishing the recovery of the sensing response by washing, we proceeded to challenge the MOF-based textile sensors using several physical and chemical tests to demonstrate the robust functional utility of the electronic textiles (Figure 5A). We chose harsh physical and chemical tests, such as heating at 120 °C for 10 min in air, heating at 120 °C for 96 h in $N_2$, abrading with a metal edge, laundering in detergent at 50 °C, ironing with steam for 60 s, and washing in 30% $H_2O_2$ for 1 min and diluted bleach for 30 min (Figures 5A and S34). Remarkably, all the devices maintained their resistance (Figure S35) and retained excellent normalized chemiresistive response to $H_2S$ at 80 ppm, indistinguishable from fresh devices (Figures 5A and S34). Analysis by PXRD confirmed that the crystallinity on $Cu_3(HHTP)_2$ MOF of cotton was largely unaffected even after the harshest physical and chemical tests (Figure S36).

We further assessed the stability of this material by analyzing the potential for copper leaching from this material in various laundering conditions via ICP-MS analysis. Under typical laundering conditions of 1 h using DI water, detergent, 1% bleach, or 30% $H_2O_2$, we observed minimal to no leaching of copper ions from the MOF/textile composite (Figure S37A); the structure of the MOF on cotton retained structural integrity, except in 30% $H_2O_2$ (Figure S37B). While soaking in water and 1% bleach for up to 24 h still did not lead to observable leaching of copper ions, soaking in detergent and 30% $H_2O_2$ led to considerable loss of copper into solution after 6 h, followed by complete MOF degradation after 24 h in concentrated hydrogen peroxide (Figure S37A,C). We rationalize the difference in leaching by the fact that highly concentrated 30% $H_2O_2$ is a known leaching agent for copper in acidic conditions,[92] while the low concentration of the bleach solution is insufficient to induce copper leaching. The detergent we used contained chelating agents, which could have contributed to the observed copper leaching.[93] Taken together, these results demonstrate exceptional stability of $Cu_3(HHTP)_2$ MOF on cotton under typical wear and laundering conditions, showing that this material degrades only under the most extreme harsh and prolonged chemical tests that should not be typically encountered in wearable devices.

Since the devices maintained their excellent sensing response to $H_2S$ after exposure to chemical tests, we proceeded to investigate device stability over multiple washing cycles of repeated tests involving submerging the devices in 30% $H_2O_2$ for 1 min, diluted bleach for 30 min (0.23% v/v), or diluted detergent for 30 min (0.23% v/v). After completion of each washing step, we activated the textile sensors in $H_2O$ for 1 h followed by acetone for 1 h. The chemiresistive devices maintained their function after multiple washing cycles (Figures 5B and S38−S40). Additional studies of analyte-specific reusability will be needed for practical implementation of MOF/textile composites in repeated chemical sensing.

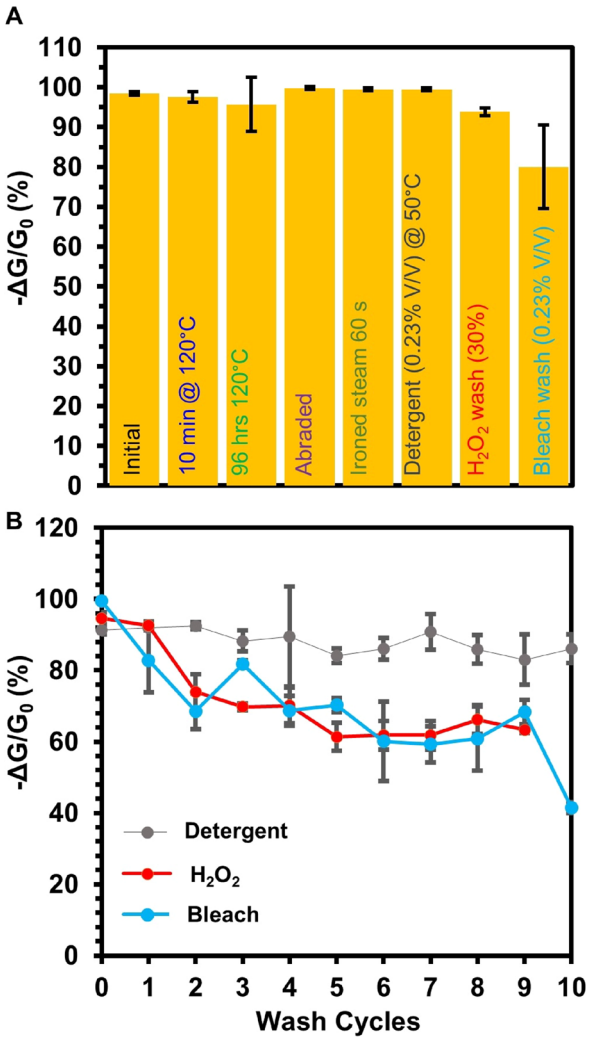


**Figure 5.** (A) Bar graph representing normalized chemiresistive response of $Cu_3(HHTP)_2$ on cotton for the detection of $H_2S$ at 80 ppm. The designated physical or chemical stresses were applied before the $Cu_3(HHTP)_2$ on cotton devices were exposed to 80 ppm $H_2S$. Each bar represents the normalized average sensing response after each respective physical or chemical stability test ($n \geq 3$). The error bars represent the standard deviation from the mean based on three or more independent measurements. (B) Sensing performance of $Cu_3(HHTP)_2$ on cotton as chemiresistors when exposed to $H_2S$ over 10 washing cycles in detergent (washing cycle = 30 min), hydrogen peroxide ($H_2O_2$) (washing cycle = 1 min), or 1% bleach in $H_2O$ (washing cycle = 30 min). Error bars represent the standard deviation from the mean based on three or more independent measurements.

**Formation of $Cu_3(HHTP)_2$ on Cotton via Oxidative Restructuring Was more Robust and Uniform Compared to the Solvothermal Method.** Comparison of the oxidative restructuring method with the previously reported


https://doi.org/10.1021/jacs.2c05510
J. Am. Chem. Soc. 2022, 144, 23297−23312

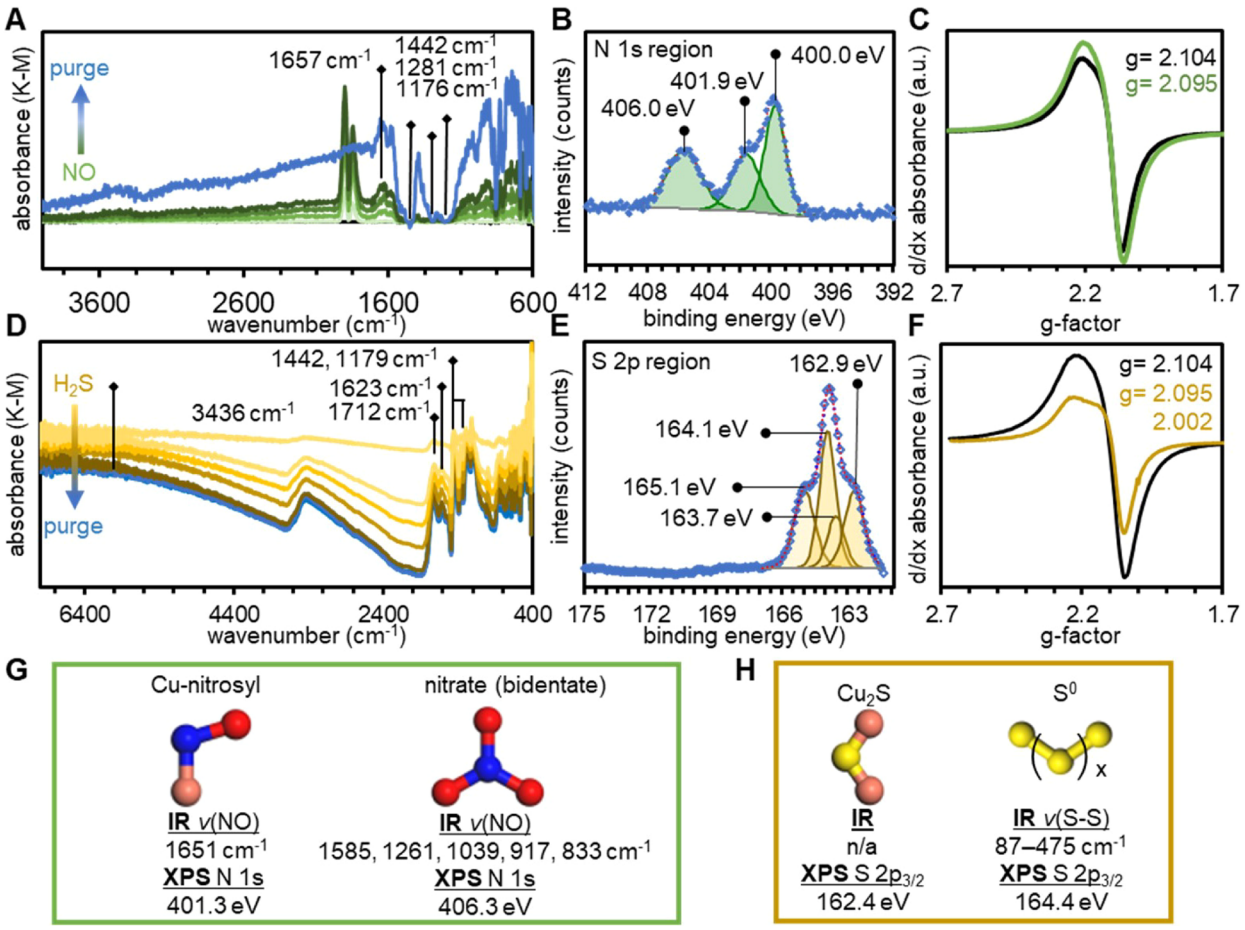


**Figure 6.** $Cu_3(HHTP)_2$ exposed to 1% NO (balance $N_2$) at 25 °C for 9 min observed by (A) DRIFTS, (B) XPS, and (C) EPR (77 K) spectroscopies. $Cu_3(HHTP)_2$ exposed to 1% $H_2S$ (balance $N_2$) at 25 °C for 20 min observed by (D) DRIFTS, (E) XPS, and (F) EPR (77 K) spectroscopies. (G) Expected FTIR and XPS spectral features of species resulting from the detoxification by adsorption or oxidation of NO over $Cu_3(HHTP)_2$. (H) Expected spectral features for FTIR and XPS of species resulting from the detoxification by adsorption or oxidation of $H_2S$ over $Cu_3(HHTP)_2$.

solvothermal or SOFT method of forming $Cu_3(HHTP)_2$ on cotton with PXRD, SEM, and other analyses (Figure S41) revealed two distinct differences between the two methods. First, the deposition of $Cu_3(HHTP)_2$ on cotton led to the formation of conductive textiles (Table S8), while the growth of the same MOF on cotton using the solvothermal method did not impart measurable conductivity on the textile substrates (resistance > 40 MΩ). We attribute this difference to the dense packing, uniformity, and preferential orientation of crystallites of this MOF on cotton promoted by the oxidative restructuring method, in contrast to the solvothermal method (Figure S41). This result demonstrates that the oxidative restructuring method was advantageous for producing electronic textiles of $Cu_3(HHTP)_2$ MOF that could be employed for chemiresistive sensing. Second, oxidative restructuring produced more robust and uniform coatings compared to the solvothermal method. The optical image of $Cu_3(HHTP)_2$ MOF on cotton formed using the SOFT method displayed fraying at the edges of the swatch, possibly due to the acidity of the reaction (pH = 4.50), whereas $Cu_3(HHTP)_2$ MOF on cotton using the oxidative restructuring method did not display fraying possibly because the reaction conditions were not as acidic (pH = 5.7) (Figure S41B).

**Micro-Breakthrough Experiments for the Filtration of $H_2S$ Using $Cu_3(HHTP)_2$ MOFs.** Micro-breakthrough experiments were conducted using the apparatus previously demonstrated by Yaghi and coworkers, which uses a rapid nanoporous adsorbent breakthrough testing apparatus.[94] In the apparatus, $H_2S$ was mixed in a carrier gas stream and passed over a temperature-controlled sorbent bed composed of the bulk synthesized $Cu_3(HHTP)_2$. In all the breakthrough studies, the effluent stream of gas passed through a Fourier transform infrared detector to determine the drop in concentration of the adsorbent target.[94] The adsorption of $H_2S$ using $Cu_3(HHTP)_2$ was classified through micro-breakthrough analysis (Figure S48). The uptake capacity of $H_2S$ with $Cu_3(HHTP)_2$ bulk powder in dry conditions (RH < 1%), determined by dynamic loading calculation, was 4.6 mol/$kg_{MOF}$. The uptake capacity of $H_2S$ in humid conditions (RH = 80%) decreased to 2.7 mol/$kg_{MOF}$. The uptake capacity of $H_2S$ using other MOFs ranges from 0.05 to 5.0 mol/$kg_{MOF}$.[88,95,96] The uptake capacity of $H_2S$ with $Cu_3(HHTP)_2$ is comparable to some benchmark MOF materials, MIL-53(Cr, Al, Fe) (3.02 mol $kg^{-1}$), Mg-CUK-1 MOF (3.10 mol/$kg_{MOF}$), and MOF-74(Ni) (4.98 mol/$kg_{MOF}$).[88,95,96] In contrast to previous results, this report constitutes the first characterization of a conductive MOF for $H_2S$ uptake.


https://doi.org/10.1021/jacs.2c05510
J. Am. Chem. Soc. 2022, 144, 23297−23312

**Spectroscopic Identification of Chemical Sensing and Detoxification Mechanisms of NO and $H_2S$ on $Cu_3(HHTP)_2$ MOF Powder.** Chemical sensing performed as part of this study indicated that the $Cu_3(HHTP)_2$ MOF has promise in removing toxic gases NO and $H_2S$ from airstreams. In order to investigate the processes of chemical detection and potential for detoxification further, we used a suite of spectroscopic techniques including diffuse reflectance infrared Fourier transform spectroscopy (DRIFTS), XPS, electron paramagnetic resonance (EPR), and PXRD to assess chemical and structural changes induced by material−analyte interactions with NO and $H_2S$.

**Spectroscopic Assessment of the Interaction between $NO_x$ and $Cu_3(HHTP)_2$.** The first method we used to investigate the interaction between NO and $Cu_3(HHTP)_2$ was DRIFTS (Figure 6A). Difference spectra revealed three key spectroscopic features upon exposure to NO and subsequent purging. First, a broad band at 1651 $cm^{-1}$ was observed after NO exposure and was irreversible after purging with $N_2$.[97] This band was assigned to NO binding to Cu centers or NO reacting with organic protons of the framework to form R-NO nitroso compounds. Second, a series of bands (1585, 1261, 1039, 917, and 833 $cm^{-1}$) (Figure S54) indicated the presence of more oxidized nitrate species most likely adsorbed in a variety of bidentate configurations to Cu centers (Figure 6G).[98] Third, the background absorbance increased during exposure to NO and increased further when the sample was purged with $N_2$. Overlaid with the positive-going background absorbance was a series of negative going bands that aligned with bands observed for pristine $Cu_3(HHTP)_2$.[64] This background absorbance probably originated from electronic features of the material.[64]

XPS spectroscopy of $Cu_3(HHTP)_2$ after exposure to NO showed the presence of new N-containing oxides of nitrogen ($NO_x$), which was consistent with results obtained by DRIFTS. The presence of a low binding energy component (400.0 eV) could originate from Cu-NO species, as indicated from DRIFTS data (Figure 6B,G). However, the location of this component of the N 1s emission line was lower than those typically associated with M-NO and may therefore also originate from organic nitroso compounds such as HHTP-NO. In addition to new emission lines from captured or converted analyte, analysis of the Cu $2p_{3/2}$ emission line showed that NO caused a redox shift of Cu within the framework from 69% $Cu^{2+}$ in the pristine state (Figure S9) to 95 $Cu^{2+}$ after exposure to NO (Figure S49E). X-band EPR spectroscopy agreed with the shift in redox balance within the framework observed by XPS (Figure 6C). Upon exposure to NO, the absorbance feature attributed to $Cu^{2+}$ ($d^9$ S = 1/2) increased in intensity, suggesting an increase in the prevalence of $Cu^{2+}$ species.

The large change in redox balance within the framework prompted us to investigate structural changes that may result from analyte exposure. PXRD diffractograms were gathered for bulk $Cu_3(HHTP)_2$ powder and for $Cu_3(HHTP)_2$ oxidatively restructured onto cotton (Figures S56 and S57). For $Cu_3(HHTP)_2$ in the bulk form, NO yielded minimal changes in the diffractogram (Figures S56 and S57). Exposure to $NO_2$ as the analyte caused large changes in diffraction peak intensity, with all diffraction peaks appearing to increase in intensity in comparison to the (100) peak. On cotton substrates, $Cu_3(HHTP)_2$ was more susceptible to changes in crystallinity due to analyte exposure. Exposure to 10,000 ppm of NO or $NO_2$ caused significant reduction in crystallinity for $Cu_3(HHTP)_2$, while also changing the diffraction peaks associated with cotton. At 40 ppm, neither analyte caused significant changes in the PXRD of $Cu_3(HHTP)_2$ on cotton (Figures S56 and S57).

**Transformation and Capture of NO within $Cu_3(HHTP)_2$.** DRIFTS and XPS identified the oxidation of NO to $NO_x$ as the primary fate of NO interacting with $Cu_3(HHTP)_2$. Both methods also identified NO bound to Cu centers. We proposed that the formation of $NO_x$, such as $NO_3^-$, in our system proceeded according to a mechanism reminiscent of the biologically relevant pathway

$$NO^{\cdot} + O_{2ads} + e^- \xrightarrow{k_1} ONOO^- \xrightarrow{k_2} NO_3^- \quad (1)$$

The electrons consumed in the process of eq 1 could be delivered by the $Cu^+$ to $Cu^{2+}$ transformation evidenced by XPS and EPR spectroscopy, or by the oxidation of HHTP ligands within the framework. Oxidation of the framework that we observed spectroscopically was paired with a chemiresistive decrease in resistance of the MOF device. This response matches with the putative p-type semi-conductivity of polycrystalline powders of $Cu_3(HHTP)_2$ observed by us and others.[56,63,99,100]

The oxidative or reductive transformation of NO to more easily captured or less toxic products has been deeply studied on supported catalysts, such as noble metals, metal oxides, and carbon-based surfaces. These reactions, such as the $NO_x$ storage reduction using Pt-Pd catalysts, are typically carried out at temperatures of 250−300 °C to access NO conversion to $NO_2$ at more than 95% in flow.[101,102] Recently, mechanisms for the disproportionation of NO on Fe and Cu centers within insulating MOFs have been discovered by Dincă and coworkers.[103,104] This report demonstrated the disproportionation of NO at room temperature over a Cu center with the ability to thermally cycle the MOF-based system to complete the catalytic cycle.[104] Our report identifies an alternative reaction pathway for NO interactions with a MOF and is the first report on NO reactions at the surface of a conductive MOF. We identify products and reaction pathways that govern the ability of $Cu_3(HHTP)_2$ to detect and decontaminate NO in air. The distinct differences in reaction pathways observed for $Cu_3(HHTP)_2$ compared to other MOFs with isolated metal sites are most likely due to the ability of the studied system to participate in redox reactions (donate electrons to the reduction of $O_2$, eq 1) and adsorb $O_2$ needed for the NO → $NO_x^-$ transformation.

**Spectroscopic Features of the Interaction between $H_2S$ and $Cu_3(HHTP)_2$.** The irreversibility of the chemiresistive sensing experiments and the ability of $Cu_3(HHTP)_2$ to purify $H_2S$ demonstrated by breakthrough studies lead us to hypothesize that strong and irreversible interactions were occurring between the probe gas and MOF substrate. To test this hypothesis, we used a series of in situ and ex situ spectroscopic techniques to investigate the interaction of $Cu_3(HHTP)_2$ powder samples with 1% $H_2S$ (balance $N_2$). In situ DRIFTS spectra during a 30 min exposure to $H_2S$ and subsequent purging with $N_2$ revealed three new spectral features (Figure 6D and Section 11.5.). First, the background absorbance of the material decreased across the broad range 6000−500 $cm^{-1}$ (Figure 6D). Second, a new broad and strong absorbance band was observed at 3436 $cm^{-1}$ (Figure 6D). The strong band at 3436 $cm^{-1}$ and the weaker band at 1623 $cm^{-1}$


https://doi.org/10.1021/jacs.2c05510
J. Am. Chem. Soc. 2022, 144, 23297−23312

were assigned to the stretching and bending modes of surface-adsorbed $H_2O$, respectively.[64] Third, a complex set of new absorbance bands was observed between 1800 and 800 $cm^{-1}$ with prominent features at 1712, 1623, 1442, 1176, and 994 $cm^{-1}$ (Figure 6D). The new band at 1712 $cm^{-1}$ was in the region typically assigned to carbonyl stretching vibrations. The similarity in energy and shape of this band to a band observed in pristine HHTP prompted us to assign this band to $\nu$(C═O) of HHTP in an oxidized state.[64] The absorbance band at 1442 $cm^{-1}$ and the less prominent features between 1400−1100 $cm^{-1}$ were similar to those we observed in our previous report of the host−guest interactions between $NH_3$ and $Cu_3(HHTP)_2$ and coincided well with bands observed for HHTP.[64] Their appearance in the difference spectra indicated that non-coordinated ligand vibrational modes were becoming more prominent with the introduction of $H_2S$. No definitive bands associated with S-containing species (e.g., $H_2S$, $SO_2$, $SO_4^{2-}$, etc.) could be identified from these spectra. The spectral features that were observed continued to increase in intensity over the course of the 28 min experiment. The changes in the difference spectra we observed after addition of $H_2S$ were irreversible after $H_2S$ was removed, indicating an irreversible transformation of the analyte and/or material.

Investigations of a similar exposure process by XPS showed that exposure to $H_2S$ induced two prominent chemical changes to $Cu_3(HHTP)_2$. First, we observed the loss of the satellite shakeup lines in the Cu 2p region, compared to the spectra of pristine $Cu_3(HHTP)_2$. We attributed this change to the quantitative reduction of spectroscopically observable $Cu^{2+}$ to either $Cu^+$ or $Cu^0$ or to the formation of CuS, which does not typically exhibit a satellite emission line.[64] Second, we observed a new emission line having four components and corresponding to two distinct chemical environments of S 2p (Figure S50).[32] Based on their binding energies, we assigned the S $2p_{3/2}$ emission line at 164.1 eV to elemental sulfur.[105] The line at 162.9 eV is 1.2 eV higher than expected for $Cu_2S$ or CuS and has been assigned to a highly Cu-deficient non-stoichiometric sulfide (Figure 6H).[106−108] The expected S $2p_{1/2}$ lines of the $S_x$ and $Cu_{2-x}S$ species accounted for the two remaining components (Figure 6E,H). EPR spectroscopy confirmed that $H_2S$ caused the conversion of EPR-active $Cu^{2+}$ to the EPR-silent species, presumably $Cu^+$ (Figure 6F).[32,41] A new organic radical was also observed in the EPR spectrum after addition of $H_2S$. This new feature correlated well with the appearance of HHTP vibrational modes observed in DRIFTS experiments after exposure to $H_2S$.

PXRD analysis of bulk $Cu_3(HHTP)_2$ after exposure to 10,000 ppm $H_2S$ revealed significant structural changes to the MOF. The structural changes to $Cu_3(HHTP)_2$ MOF were indicated by an increase in intensity of the (200) and (002) peaks relative to the intensity of the (100) diffraction peak. New diffraction peaks were observed at 33 and 48° 2$\theta$, which could correspond to the (103) plane and (110) planes of copper sulfide, respectively (Figure S58A).[109] $Cu_3(HHTP)_2$ on cotton upon exposure to 10,000 ppm $H_2S$ showed a reduction in crystallinity based on the significant broadening of peaks in the (100) and (200) diffraction peaks (Figure S58B) and a sharp peak at 22° 2$\theta$ similar to elemental sulfur. Analysis of the MOF on cotton by PXRD after saturation with $H_2S$ at 40 ppm showed minimal structural changes (Figure S58C), indicating that the copper sulfide particles observed in XPS are too small or too poorly ordered to be observed in PXRD.

**Transformation and Capture of $H_2S$ within $Cu_3(HHTP)_2$.** Spectroscopic investigations confirmed the strong and irreversible interaction between $H_2S$ and $Cu_3(HHTP)_2$ inferred from chemiresistive sensing and breakthrough studies. The results of our DRIFTS investigations identify the generation of water as a byproduct of the reaction between $H_2S$ and $Cu_3(HHTP)_2$. DRIFTS also revealed a set of vibrational modes that correlated well with the spectrum of pristine HHTP, suggesting that interactions between the analyte and substrate resulted in weaker metal bis(dioxolene) bonding and vibrational contributions increasingly representative of the individual components, namely, HHTP, compared to an extended framework.[64] This perturbation was consistent with EPR studies, which showed a new organic radical, presumably from HHTP. From DRIFTS evidence, we considered possible pathways of $H_2S$ detoxification. First, we considered the surface chemistry of metal edge sites within $Cu_3(HHTP)_2$, which could include copper hydroxide capping units. A well-known reaction of copper hydroxides with $H_2S$ yields water and copper sulfide,[110] which could explain both the evolution of water and the liberation of HHTP from Cu bis(dioxolene) linkages

$$Cu(OH)_2 + H_2S \rightarrow CuS + 2H_2O \quad (2)$$

However, the presence of elemental sulfur species and sulfides of copper ($Cu_yS_x$) would not be observable by IR spectroscopy.[111] We, therefore, relied on XPS to reveal the oxidation state of captured sulfur species.[110] The identification of $S_x$ and lack of observed $H_2S$ species in the S 2p region of the XPS spectra confirmed the capture and oxidation of $H_2S$ on the MOF surface. Analysis also showed formation of $Cu_yS_x$ species, which we further identified as $Cu_2S$ using the Cu 2p region[112] and the magnitude of the observed $Cu^{2+}$ (S = 1/2) absorbance by EPR.[32] Although $Cu_yS_x$ compounds typically do not exhibit shakeup emissions, instead behaving more like a metallic structure, the reduction of $Cu^{2+}$ observed by EPR[32] and the location of the S $2p_{3/2}$ emission line both indicated the presence of $Cu_2S$[113] rather than CuS.[114] We propose that the active edges ({100} family of planes) of the MOF nanorods, which dominate the exposed surface area, decorated with terminal (HHTP)Cu($OH_x$)$_y$ edge sites can undergo a reaction with $H_2S$ along the following pathway (eq 3)

$$2(HHTP)Cu(OH)_2 + 2H_2S \rightarrow 2(HHTP) + Cu_2S + 2H_2O \quad (3)$$

Our proposed modes of interaction between $H_2S$ and $Cu_3(HHTP)_2$ provide a context that accounts for the spectroscopic evidence for the observation of the formation of $Cu_2S$, $H_2O$, and $S_x$ as byproducts of detoxification. The exact pathway for how the formation of these products leads to the dramatic loss of conductivity observed in chemiresistive experiments was difficult to pinpoint. We propose three possible mechanisms. First, the oxidation of $H_2S$ and the reduction of Cu in the framework would reduce the concentration of charge carriers in the p-type semiconductor by adding electrons to the valence band of the MOF.[63] Second, the formation of $Cu_2S$ would cause degradation of the Cu bis(dioxolene) linkages reducing covalency and electronic conductivity. Related to this mechanism, the loss of mixed valency ($Cu^{2+}/Cu^+$) in the framework when Cu is fully reduced could negatively impact the conductivity of the material. Third, $S_x$ species ($x$ = 2−8) are known to be


https://doi.org/10.1021/jacs.2c05510
J. Am. Chem. Soc. 2022, 144, 23297−23312

electrically insulating and their formation on the surface of the MOFs could insulate crystallites from one another and reduce their ability to transfer charge.[115,116]

MOFs have shown great promise for $H_2S$ capture. Their high surface area and ability to provide well-dispersed metal sites are beneficial properties for adsorption-driven capture of $H_2S$.[88,117] However, rigorous spectroscopic methods have rarely been employed in the identification of adsorbed states of $H_2S$ or examination of possible chemical reactions of $H_2S$. The high reactivity of $H_2S$ and its propensity to be oxidized or disproportionate on surface[118,119] and its alacrity for formation of metal-sulfides necessitate a comprehensive set of spectroscopic tools to identify host−guest interactions and mechanisms of separation.[120] Our report presents a systematic investigation of the ability of $Cu_3(HHTP)_2$ to detect, detoxify, and filter $H_2S$.

## CONCLUSIONS

This paper demonstrates a new mild, robust, and rapid method for integration of $Cu_3(HHTP)_2$ MOF onto flexible porous substrates by restructuring $Cu^0$ features directly into MOFs capable of multifunctional performance as an e-textile sensor. This method possesses at least three innovative characteristics in the context of multifunctional e-textiles. First, oxidative restructuring advances the development of new integration strategies of MOFs ($Cu_3(HHTP)_2$) onto flexible substrates with synthetic ease and remarkable robustness. To date, there are few examples for the integration of 2D conductive MOFs to generate e-textiles, where the conductivity of the textile is imparted by the use of MOFs without conductive additives.[12,21,53] These existing examples possess limitations in terms of substrate choice and diversity of MOFs that our method overcomes. Second, e-textiles patterned with $Cu_3(HHTP)_2$ not only detect NO and $H_2S$ down to 1 ppm, but also maintain their sensing response after washing as well as harsh physical and chemical stresses. This study is the first to report a comprehensive stability test that demonstrates the promising advantage of the $Cu_3(HHTP)_2$ MOF as an exceptionally robust chemical sensor, especially when integrated with textiles. Third, we detail the first example of a spectroscopic study that provides insight into the interactions between $Cu_3(HHTP)_2$ and NO, as well as $H_2S$, indicating that chemical transformations of both gases are promoted by the presence of MOF. Taken together, these innovative characteristics illustrate that the new method of textile integration of the $Cu_3(HHTP)_2$ MOF reported herein has unprecedented robustness and multifunctional performance characteristics in the context of e-textile sensors. This study focused on the sensing and uptake of $H_2S$ and NO; however, the $Cu_3(HHTP)_2$ MOF has potential for the adsorption and detection of other gaseous threat agents due to the presence of undercoordinated copper sites.[121,122] Practical implementation of $Cu_3(HHTP)_2$ on textiles in simultaneous sensing and detoxification will require additional understanding of the selectivity and sensitivity of $Cu_3(HHTP)_2$ MOF with other toxic gases.

While oxidative restructuring enables facile, robust, and functional integration of $Cu_3(HHTP)_2$ MOF onto textiles under ambient conditions, this method currently has at least three limitations. First, the demonstration of oxidative restructuring of metals into MOF is currently limited to $Cu^0$. However, this limitation may be overcome with further development by tailoring conditions for the controlled oxidation of other transition metals through the introduction of specific oxidants and solvent systems. Second, this method relies on the use of a thermal evaporator, which restricted the patterning of Cu metal to planar processing and may be limited in scalability. The use of electroless plating of copper metal in future applications could eliminate the need for specialized equipment, enhance scalability, and overcome limitations of planar processing.[123] Third, the demonstration in this study is currently limited to the HHTP ligand. Strategic optimization of reaction conditions to make them amenable to other ligands will be required for developing broad applicability of this method.

The systematic study of conductive MOFs on porous textiles in the context of chemical detection and spectroscopic assessment illustrates the multifunctional capabilities of this class of 2D conductive MOFs, especially when coupled with robust integration onto textiles. Our fundamental insight and mechanistic details on sensing properties, surface interactions, and demonstration of the exceptional chemical stability of the $Cu_3(HHTP)_2$ MOF pave the way for the design of next-generation personal protective systems, with MOFs providing not only filtration and detoxification, but also real-time chemical detection. Oxidative restructuring as a means of installing conductive MOF materials at the fiber level could become a platform technology for producing scalable multifunctional e-textiles, which will expand the scope of Moore's Law for fibers.[10]

## ASSOCIATED CONTENT

### Supporting Information

The Supporting Information is available free of charge at https://pubs.acs.org/doi/10.1021/jacs.2c05510.

Experimental details, scanning electron microscopy, energy-dispersive X-ray spectroscopy, X-ray photoelectron spectra, powder X-ray diffraction, chemiresistive sensing data, and diffuse reflectance infrared Fourier transform spectroscopy (PDF)

## AUTHOR INFORMATION


### Corresponding Author

**Katherine A. Mirica** − *Department of Chemistry, Burke Laboratory, Dartmouth College, Hanover, New Hampshire 03755, United States;* orcid.org/0000-0002-1779-7568; Email: Katherine.A.Mirica@dartmouth.edu

### Authors

**Aileen M. Eagleton** − *Department of Chemistry, Burke Laboratory, Dartmouth College, Hanover, New Hampshire 03755, United States*

**Michael Ko** − *Department of Chemistry, Burke Laboratory, Dartmouth College, Hanover, New Hampshire 03755, United States*

**Robert M. Stolz** − *Department of Chemistry, Burke Laboratory, Dartmouth College, Hanover, New Hampshire 03755, United States;* orcid.org/0000-0002-9291-0794

**Nataliia Vereshchuk** − *Department of Chemistry, Burke Laboratory, Dartmouth College, Hanover, New Hampshire 03755, United States;* orcid.org/0000-0002-9067-3895

**Zheng Meng** − *Department of Chemistry, Burke Laboratory, Dartmouth College, Hanover, New Hampshire 03755, United States;* orcid.org/0000-0002-6775-3213




https://doi.org/10.1021/jacs.2c05510
J. Am. Chem. Soc. 2022, 144, 23297−23312

**Lukasz Mendecki** − *Department of Chemistry, Burke Laboratory, Dartmouth College, Hanover, New Hampshire 03755, United States*
**Adelaide M. Levenson** − *Department of Chemistry, Burke Laboratory, Dartmouth College, Hanover, New Hampshire 03755, United States*
**Connie Huang** − *Department of Chemistry, Burke Laboratory, Dartmouth College, Hanover, New Hampshire 03755, United States*
**Katherine C. MacVeagh** − *Department of Chemistry, Burke Laboratory, Dartmouth College, Hanover, New Hampshire 03755, United States*
**Akbar Mahdavi-Shakib** − *Department of Chemistry, Frontier Institute for Research in Sensor Technology (FIRST), University of Maine, Orono, Maine 04469, United States;* orcid.org/0000-0003-1763-6761
**John J. Mahle** − *DEVCOM Chemical Biological Center, Aberdeen Proving Ground, Maryland 21010-5424, United States*
**Gregory W. Peterson** − *DEVCOM Chemical Biological Center, Aberdeen Proving Ground, Maryland 21010-5424, United States;* orcid.org/0000-0003-3467-5295
**Brian G. Frederick** − *Department of Chemistry, Frontier Institute for Research in Sensor Technology (FIRST), University of Maine, Orono, Maine 04469, United States;* orcid.org/0000-0002-5715-6511

Complete contact information is available at: https://pubs.acs.org/10.1021/jacs.2c05510

### Author Contributions

A.M.E. and M.K. contributed equally to this work. The manuscript was written through contributions of all authors. All authors have given approval to the final version of the manuscript.

### Notes

The authors declare no competing financial interest.

## ■ ACKNOWLEDGMENTS

The authors acknowledge support from the National Science Foundation EPSCoR award (#1757371), Army Research Office Young Investigator Program Grant No. W911NF-17-1-0398, NSF CAREER award (#1945218), NIH MIRA Award (R35GM138318), Camille Dreyfus Teacher-Scholar Award, and Dartmouth College. The authors thank the University Instrumentation Center at the University of New Hampshire (Durham, NH) for the access to XPS and SEM. The authors thank Amelia W. Jackson and Ida Z. Claude for contributing to the optimization of synthetic conditions using oxidative restructuring and Lori-Ann Y. Williams and Claudia G. Durbin for contributing to the preparation of devices for control experiments. Gregory W. Peterson and John J. Mahle thank the Defense Threat Reduction Agency (Program CB3934) for funding the breakthrough work.

## ■ REFERENCES

(1) Rogers, J. A.; Someya, T.; Huang, Y. Materials and Mechanics for Stretchable Electronics. *Science* **2010**, *327*, 1603−1607.
(2) Kim, D.; Lu, N.; Ma, R.; Kim, Y.; Kim, R.; Wang, S.; Wu, J.; Won, S. M.; Islam, A.; Yu, K. J.; Kim, T.; Chowdhury, R.; Ying, M.; Xu, L.; Li, M.; Chung, H.; Keum, H.; McCormick, M.; Liu, P.; Zhang, Y.; Omenetto, F. G.; Huang, Y.; Coleman, T.; Rogers, J. A. Epidermal Electronics. *Science* **2011**, *333*, 838−843.
(3) Someya, T.; Bao, Z.; Malliaras, G. G. The Rise of Plastic Bioelectronics. *Nature* **2016**, *540*, 379−385.
(4) Xu, X.; Xie, S.; Zhang, Y.; Peng, H. The Rise of Fiber Electronics. *Angew. Chem., Int. Ed.* **2019**, *58*, 13643−13653.
(5) Zhang, Y.; Zhang, L.; Cui, K.; Ge, S.; Cheng, X.; Yan, M.; Yu, J.; Liu, H. Flexible Electronics Based on Micro/Nanostructured Paper. *Adv. Mater.* **2018**, *30*, No. 1801588.
(6) TaekJung, W.; Jeon, J. W.; Jang, H.; Kim, D. Y.; Lee, H.; Kim, B. H. Commercial Silk-Based Electronic Textiles for NO2 Sensing. *Sens. Actuators B Chem.* **2020**, *307*, No. 127596.
(7) Ma, K.; Islamoglu, T.; Chen, Z.; Li, P.; Wasson, M. C.; Chen, Y.; Wang, Y.; Peterson, G. W.; Xin, J. H.; Farha, O. K. Scalable and Template-Free Aqueous Synthesis of Zirconium-Based Metal-Organic Framework Coating on Textile Fiber. *J. Am. Chem. Soc.* **2019**, *141*, 15626−15633.
(8) Giannakoudakis, D. A.; Hu, Y.; Florent, M.; Bandosz, T. J. Smart Textiles of MOF/g-$C_3N_4$ Nanospheres for the Rapid Detection/Detoxification of Chemical Warfare Agents. *Nanoscale Horiz.* **2017**, *2*, 356−364.
(9) Rein, M.; Favrod, V. D.; Hou, C.; Khudiyev, T.; Stolyarov, A.; Cox, J.; Chung, C.; Chhav, C.; Ellis, M.; Joannopoulos, J.; Fink, Y. Diode Fibres for Fabric-Based Optical Communications. *Nature* **2018**, *560*, 214−218.
(10) Loke, G.; Alain, J.; Yan, W.; Khudiyev, T.; Noel, G.; Yuan, R.; Missakian, A.; Fink, Y. Computing Fabrics. *Matter* **2020**, *2*, 786−788.
(11) Loke, G.; Khudiyev, T.; Wang, B.; Fu, S.; Payra, S.; Shaoul, Y.; Fung, J.; Chatziveroglou, I.; Chou, P.; Chinn, I.; Yan, W.; Gitelson-Kahn, A.; Joannopoulos, J.; Fink, Y. Digital Electronics in Fibres Enable Fabric-Based Machine-Learning Inference. *Nat. Commun.* **2021**, *12*, 3317.
(12) Smith, M. K.; Mirica, K. A. Self-Organized Frameworks on Textiles (SOFT): Conductive Fabrics for Simultaneous Sensing, Capture, and Filtration of Gases. *J. Am. Chem. Soc.* **2017**, *139*, 16759−16767.
(13) Rauf, S.; Vijapu, M. T.; Andrés, M. A.; Gascón, I.; Roubeau, O.; Eddaoudi, M.; Salama, K. N. Highly Selective Metal−Organic Framework Textile Humidity Sensor. *ACS Appl. Mater. Interfaces* **2020**, *12*, 29999−30006.
(14) Lee, D. T.; Zhao, J.; Peterson, G. W.; Parsons, G. N. Catalytic "MOF-Cloth" Formed via Directed Supramolecular Assembly of UiO-66-NH2 Crystals on Atomic Layer Deposition-Coated Textiles for Rapid Degradation of Chemical Warfare Agent Simulants. *Chem. Mater.* **2017**, *29*, 4894−4903.
(15) Barton, H. F.; Jamir, J. D.; Davis, A. K.; Peterson, G. W.; Parsons, G. N. Doubly Protective MOF-Photo-Fabrics: Facile Template-Free Synthesis of PCN-222-Textiles Enables Rapid Hydrolysis, Photo-Hydrolysis and Selective Oxidation of Multiple Chemical Warfare Agents and Simulants. *Chem. − Eur. J.* **2021**, *27*, 1465−1472.
(16) Lee, D. T.; Jamir, J. D.; Peterson, G. W.; Parsons, G. N. Protective Fabrics: Metal-Organic Framework Textiles for Rapid Photocatalytic Sulfur Mustard Simulant Detoxification. *Matter* **2020**, *2*, 404−415.
(17) de Koning, M. C.; Ma, K.; van Grol, M.; Iordanov, I.; Kruijne, M. J. L.; Idrees, K. B.; Xie, H.; Islamoglu, T.; Bross, R. P. T.; Farha, O. K. Development of a Metal−Organic Framework/Textile Composite for the Rapid Degradation and Sensitive Detection of the Nerve Agent VX. *Chem. Mater.* **2022**, *34*, 1269−1277.
(18) Nie, X.; Wu, S.; Huang, F.; Wang, Q.; Wei, Q. Smart Textiles with Self-Disinfection and Photothermochromic Effects. *ACS Appl. Mater. Interfaces* **2021**, *13*, 2245−2255.
(19) Kim, J.; Kumar, R.; Bandodkar, A. J.; Wang, J. Advanced Materials for Printed Wearable Electrochemical Devices: A Review. *Adv. Electron. Mater.* **2017**, *3*, No. 1600260.
(20) Singha, K.; Kumar, J.; Pandit, P. Recent Advancements in Wearable & Smart Textiles: An Overview. *Mater. Today: Proc.* **2019**, *16*, 1518−1523.
(21) Lee, H.; Jeon, S. Polyacrylonitrile Nanofiber Membranes Modified with Ni-Based Conductive Metal Organic Frameworks for

Air Filtration and Respiration Monitoring. *ACS Appl. Nanomater.* **2020**, *3*, 8192−8198.
(22) Rabiee, N.; Bagherzadeh, M.; Ghasemi, A.; Zare, H.; Ahmadi, S.; Fatahi, Y.; Dinarvand, R.; Rabiee, M.; Ramakrishna, S.; Shokouhimehr, M.; Varma, R. S. Point-of-Use Rapid Detection of SARS-CoV-2: Nanotechnology-Enabled Solutions for the COVID-19 Pandemic. *Int. J. Mol. Sci.* **2020**, *21*, 5126.
(23) Ma, S.; Zhang, M.; Nie, J.; Yang, B.; Song, S.; Lu, P. Multifunctional Cellulose-Based Air Filters with High Loadings of Metal−Organic Frameworks Prepared by in Situ Growth Method for Gas Adsorption and Antibacterial Applications. *Cellulose* **2018**, *25*, 5999−6010.
(24) Li, P.; Li, J.; Feng, X.; Li, J.; Hao, Y.; Zheng, J.; Wang, H.; Yin, A.; Zhou, J.; Ma, X.; Wang, B. Metal-Organic Frameworks with Photocatalytic Bactericidal Activity for Integrated Air Cleaning. *Nat. Commun.* **2019**, *10*, 2177.
(25) Jost, K.; Dion, G.; Gogotsi, Y. Textile Energy Storage in Perspective. *J. Mater. Chem. A* **2014**, *2*, 10776−10787.
(26) Stoppa, M.; Chiolerio, A. Wearable Electronics and Smart Textiles: A Critical Review. *Sensors* **2014**, *14*, 11957−11992.
(27) Heikenfeld, J.; Jajack, A.; Rogers, J.; Gutruf, P.; Tian, L.; Pan, T.; Li, R.; Khine, M.; Kim, J.; Wang, J.; Kim, J. Wearable Sensors: Modalities, Challenges, and Prospects. *Lab Chip* **2018**, *18*, 217−248.
(28) Wanwong, S.; Sangkhun, W.; Homayounfar, S. Z.; Park, K.; Andrew, T. L. Wash-Stable, Oxidation Resistant Conductive Cotton Electrodes for Wearable Electronics. *RSC Adv.* **2019**, *9*, 9198−9203.
(29) Han, J.; Kim, B.; Li, J.; Meyyappan, M. A Carbon Nanotube Based Ammonia Sensor on Cotton Textile. *Appl. Phys. Lett.* **2013**, *102*, 193104.
(30) Hong, K. H.; Kyung, O. K. W.; Kang, T. J. Polyaniline−Nylon 6 Composite Fabric for Ammonia Gas Sensor. *J. Appl. Polym. Sci.* **2004**, *92*, 37−42.
(31) Mendecki, L.; Mirica, K. A. Conductive Metal−Organic Frameworks as Ion-to-Electron Transducers in Potentiometric Sensors. *ACS Appl. Mater. Interfaces* **2018**, *10*, 19248−19257.
(32) Meng, Z.; Aykanat, A.; Mirica, K. A. Welding Metallophthalocyanines into Bimetallic Molecular Meshes for Ultrasensitive, Low-Power Chemiresistive Detection of Gases. *J. Am. Chem. Soc.* **2019**, *141*, 2046−2053.
(33) Campbell, M. G.; Liu, S. F.; Swager, T. M.; Dincă, M. Chemiresistive Sensor Arrays from Conductive 2D Metal−Organic Frameworks. *J. Am. Chem. Soc.* **2015**, *137*, 13780−13783.
(34) Rubio-Giménez, V.; Galbiati, M.; Castells-Gil, J.; Almora-Barrios, N.; Navarro-Sánchez, J.; Escorcia-Ariza, G.; Mattera, M.; Arnold, T.; Rawle, J.; Tatay, S.; Coronado, E.; Martí-Gastaldo, C. Bottom-Up Fabrication of Semiconductive Metal-Organic Framework Ultrathin Films. *Adv. Mater.* **2018**, *30*, No. 1704291.
(35) Day, R. W.; Bediako, D. K.; Rezaee, M.; Parent, L. R.; Skorupskii, G.; Arguilla, M. Q.; Hendon, C. H.; Stassen, I.; Gianneschi, N. C.; Kim, P.; Dincă, M. Single Crystals of Electrically Conductive Two-Dimensional Metal−Organic Frameworks: Structural and Electrical Transport Properties. *ACS Cent. Sci.* **2019**, *5*, 1959−1964.
(36) Miner, E. M.; Fukushima, T.; Sheberla, D.; Sun, L.; Surendranath, Y.; Dincă, M. Electrochemical Oxygen Reduction Catalysed by $Ni_3$(Hexaiminotriphenylene)$_2$. *Nat. Commun.* **2016**, *7*, 10942.
(37) Zhao, M.; Huang, Y.; Peng, Y.; Huang, Z.; Ma, Q.; Zhang, H. Two-Dimensional Metal−Organic Framework Nanosheets: Synthesis and Applications. *Chem. Soc. Rev.* **2018**, *47*, 6267−6295.
(38) Clough, A. J.; Woo, J. W.; Mecklenberg, M. H.; Marinescu, S. C. Two-Dimensional Metal−Organic Surfaces for Efficient Hydrogen Evolution from Water. *J. Am. Chem. Soc.* **2015**, *137*, 118−121.
(39) Sheberla, D.; Bachman, J. C.; Elias, J. S.; Sun, C.; Shao-Horn, Y.; Dincă, M. Conductive MOF Electrodes for Stable Supercapacitors with High Areal Capacitance. *Nat. Mater.* **2017**, *16*, 220−224.
(40) Ko, M.; Mendecki, L.; Mirica, K. A. Conductive Two-Dimensional Metal−Organic Frameworks as Multifunctional Materials. *Chem. Commun.* **2018**, *54*, 7873−7891.
(41) Hmadeh, M.; Lu, Z.; Liu, Z.; Gándara, F.; Furukawa, H.; Wan, S.; Augustyn, V.; Chang, R.; Liao, L.; Zhou, F.; Perre, E.; Ozolins, V.; Suenaga, K.; Duan, X.; Dunn, B.; Yamamto, Y.; Terasaki, O.; Yaghi, O. M. New Porous Crystals of Extended Metal-Catecholates. *Chem. Mater.* **2012**, *24*, 3511−3513.
(42) Yang, S.; Wang, Y.; Yu, Y.; Bian, S. Flexible Polyester Yarn/Au/Conductive Metal-Organic Framework Composites for Yarn-Shaped Supercapacitors. *J. Electroanal. Chem.* **2019**, *847*, No. 113218.
(43) Zhou, S.; Kong, X.; Zeng, B.; Huo, F.; Strømme, M.; Xu, C. Cellulose Nanofiber @ Conductive Metal−Organic Frameworks for High-Performance Flexible Supercapacitors. *ACS Nano* **2019**, *13*, 9578−9586.
(44) Zhang, B.; Chen, H.; Hu, Q.; Jiang, L.; Shen, Y.; Zhao, D.; Zhou, Z. CelluMOFs: Green, Facile, and Flexible Metal-Organic Frameworks for Versatile Applications. *Adv. Funct. Mater.* **2021**, *31*, No. 2105395.
(45) Ma, K.; Idrees, K. B.; Son, F. A.; Maldanado, R.; Wasson, M. C.; Wang, X.; Wang, X.; Shehayeb, E.; Merhi, A.; Kaafarani, B. R.; Islamoglu, T.; Xin, J. H.; Farha, O. K. Fiber Composites of Metal−Organic Frameworks. *Chem. Mater.* **2020**, *32*, 7120−7140.
(46) Peterson, G. W.; Lee, D. T.; Barton, H. F.; Epps, T. H.; Parsons, G. N. Fibre-Based Composites from the Integration of Metal−Organic Frameworks and Polymers. *Nat. Rev. Mater.* **2021**, *6*, 605−621.
(47) Emam, H. E.; Abdelhameed, R. M. Anti-UV Radiation Textiles Designed by Embracing with Nano-MIL (Ti, In)−Metal Organic Framework. *ACS Appl. Mater. Interfaces* **2017**, *9*, 28034−28045.
(48) Emam, H. E.; Abdelhamid, H. N.; Abdelhameed, R. M. Self-Cleaned Photoluminescent Viscose Fabric Incorporated Lanthanide-Organic Framework (Ln-MOF). *Dyes Pigm.* **2018**, *159*, 491−498.
(49) Abdelhamid, H. N.; Mathew, A. P. Cellulose−Metal Organic Frameworks (CelloMOFs) Hybrid Materials and Their Multifaceted Applications: A Review. *Coord. Chem. Rev.* **2022**, *451*, No. 214263.
(50) Bian, L.; Dong, Y.; Jiang, B. Simplified Creation of Polyester Fabric Supported Fe-Based MOFs by an Industrialized Dyeing Process: Conditions Optimization, Photocatalytics Activity and Polyvinyl Alcohol Removal. *J. Environ. Sci.* **2022**, *116*, 52−67.
(51) Zhang, Y.; Jia, Y.; Hou, L. Synthesis of Zeolitic Imidazolate Framework-8 on Polyester Fiber for PM2.5 Removal. *RSC Adv.* **2018**, *8*, 31471−31477.
(52) Kundu, T.; Garai, B.; Kaskel, S. Natural Polymer-Based MOF Composites. In *Metal-Organic Frameworks in Biomedical and Environmental Field*; Springer, 2021; pp. 321−348.
(53) Lee, D. T.; Jamir, J. D.; Peterson, G. W.; Parsons, G. N. Water-Stable Chemical-Protective Textiles via Euhedral Surface-Oriented 2D Cu-TCPP Metal-Organic Frameworks. *Small* **2019**, *15*, No. 1805133.
(54) Zhao, J.; Gong, B.; Nunn, W. T.; Lemaire, P. C.; Stevens, E. C.; Sidi, F. I.; Williams, P. S.; Oldham, C. J.; Walls, H. J.; Shepherd, S. D.; Browe, M. A.; Peterson, G. W.; Losego, M. D.; Parsons, G. N. Conformal and Highly Adsorptive Metal−Organic Framework Thin Films via Layer-by-Layer Growth on ALD-Coated Fiber Mats. *J. Mater. Chem. A* **2015**, *3*, 1458−1464.
(55) Kalaj, M.; Denny, M. S., Jr.; Bentz, K. C.; Palomba, J. M.; Cohen, S. M. Nylon−MOF Composites through Postsynthetic Polymerization. *Angew. Chem. Int. Ed.* **2019**, *131*, 2358−2362.
(56) Smith, M. K.; Jensen, K. E.; Pivak, P. A.; Mirica, K. A. Direct Self-Assembly of Conductive Nanorods of Metal−Organic Frameworks into Chemiresistive Devices on Shrinkable Polymer Films. *Chem. Mater.* **2016**, *28*, 5264−5268.
(57) Li, W.; Ding, K.; Yao, M.; Nath, B.; Deng, W.; Wang, Y.; Xu, G. Conductive Metal−Organic Framework Nanowire Array Electrodes for High-Performance Solid-State Supercapacitors. *Adv. Funct. Mater.* **2017**, *27*, No. 1702067.
(58) Yim, C.; Abuzalat, O.; Elsayed, M.; Park, S.; Kim, S. Rapid Fabrication of Metal−Organic Framework Films from Metal Substrates Using Intense Pulsed Light. *Cryst. Growth Des.* **2018**, *18*, 6946−6955.
(59) Liu, T.; Liu, Y.; Xu, J.; Yao, L.; Liu, D.; Wang, C. Conversion of $Cu_2O$ Nanowires into $Cu_2O$/HKUST-1 Core/Sheath Nanostructures

and Hierarchical HKUST-1 Nanotubes. *RSC Adv.* **2016**, *6*, 91440−91444.
(60) Ji, H.; Hwang, S.; Kim, K.; Kim, C.; Jeong, N. C. Direct in Situ Conversion of Metals into Metal−Organic Frameworks: A Strategy for the Rapid Growth of MOF Films on Metal Substrates. *ACS Appl. Mater. Interfaces* **2016**, *8*, 32414−32420.
(61) Okada, K.; Ricco, R.; Tokudome, Y.; Styles, M. J.; Hill, A. J.; Takahashi, M.; Falcaro, P. Copper Conversion into $Cu(OH)_2$ Nanotubes for Positioning $Cu_3(BTC)_2$ MOF Crystals: Controlling the Growth on Flat Plates, 3D Architectures, and as Patterns. *Adv. Funct. Mater.* **2014**, *24*, 1969−1977.
(62) de Lourdes Gonzalez-Juarez, M.; Flores, E.; Martin-Gonzalez, M.; Nandhakumar, I.; Bradshaw, D. Electrochemical Deposition and Thermoelectric Characterisation of a Semiconducting 2-D Metal−Organic Framework Thin Film. *J. Mater. Chem. A* **2020**, *8*, 13197−13206.
(63) Ko, M.; Aykanat, A.; Smith, M. K.; Mirica, K. A. Drawing Sensors with Ball-Milled Blends of Metal-Organic Frameworks and Graphite. *Sensors* **2017**, *17*, 2192.
(64) Stolz, R. M.; Mahdavi-Shakib, A.; Frederick, B. G.; Mirica, K. A. Host−Guest Interactions and Redox Activity in Layered Conductive Metal−Organic Frameworks. *Chem. Mater.* **2020**, *32*, 7639−7652.
(65) Cychosz, K. A.; Thommes, M. Progress in the Physisorption Characterization of Nanoporous Gas Storage Materials. *Engineering* **2018**, *4*, 559−566.
(66) Zhao, J.; Li, X.; Li, X.; Cai, Z.; Ge, F. A Flexible Carbon Electrode Based on Traditional Cotton Woven Fabrics with Excellent Capacitance. *J. Mater. Sci.* **2017**, *52*, 9773−9779.
(67) Kuhr, M.; Aibibu, D.; Cherif, C. Targeted Partial Finishing of Barrier Textiles with Microparticles, and Their Effects on Barrier Properties and Comfort. *J. Ind. Text.* **2016**, *45*, 853−878.
(68) Ninawe, P.; Gupta, K.; Ballav, N. Chemically Integrating a 2D Metal−Organic Framework with 2D Functionalized Graphene. *Inorg. Chem.* **2021**, *60*, 19079−19085.
(69) Burkstrand, J. M. Metal-polymer Interfaces: Adhesion and X-ray Photoemission Studies. *J. Appl. Phys.* **1981**, *52*, 4795−4800.
(70) Root, W.; Wright, T.; Caven, B.; Bechtold, T.; Pham, T. Flexible Textile Strain Sensor Based on Copper-Coated Lyocell Type Cellulose Fabric. *Polymer* **2019**, *11*, 784.
(71) Esteve-Turrillas, F. A.; de la Guardia, M. Environmental Impact of Recover Cotton in Textile Industry. *Resour. Conserv. Recycl.* **2017**, *116*, 107−115.
(72) Scherzer, M.; Girgsdies, F.; Stotz, E.; Willinger, M.; Frei, E.; Schlögl, R.; Pietsch, U.; Lunkenbein, T. Electrochemical Surface Oxidation of Copper Studied by in Situ Grazing Incidence X-Ray Diffraction. *J. Phys. Chem. C* **2019**, *123*, 13253−13262.
(73) Reinhardt, K. A.; Reidy, R. F. *Handbook of Cleaning in Semiconductor Manufacturing: Fundamental and Applications*; Wiley-Scrivener Publishing LLC, 2010.
(74) Gomez-Herrero, A. C.; Sanchez-Sanchez, C.; Cherioux, F.; Martınez, J. I.; Abad, J.; Floreano, L.; Verdini, A.; Cossaro, A.; Mazaleyrat, E.; Valerie Guisset, V.; David, P.; Lisi, S.; Gago, J. A. M.; Coraux, J. Copper-Assisted Oxidation of Catechols into Quinone Derivatives. *Chem. Sci.* **2021**, *12*, 2257.
(75) Barthram, A. M.; Cleary, R. L.; Kowallick, R.; Ward, M. D. A New Redox-Tunable near-IR Dye Based on a Trinuclear Ruthenium (II) Complex of Hexahydroxytriphenylene. *Chem. Commun.* **1998**, 2695−2696.
(76) Zhang, Q.; Zhu, Z.; Liu, P.; Zhang, J.; Cao, F. Corrosion Electrochemical Kinetic Study of Copper in Acidic Solution Using Scanning Electrochemical Microscopy. *J. Electrochem. Soc.* **2019**, *166*, C401−C409.
(77) Nutting, J. E.; Gerken, J. B.; Stamoulis, A. G.; Bruns, D. L.; Stahl, S. S. "How Should I Think about Voltage? What Is Overpotential?": Establishing an Organic Chemistry Intuition for Electrochemistry. *J. Org. Chem.* **2021**, *86*, 15875−15885.
(78) Zumdahl, S. S.; Zumdahl, S. A. *Chemistry*; Houghton Mifflin Company: Boston, New York, 2007; p. A25.
(79) de Gromboy, T. S.; Shreir, L. L. The Formation of Nickel Oxides During the Passivation of Nickel in Nickel Oxides During the Passivation of Nickel in Relation to the Potential/pH Diagram*. *Electrochim. Acta* **1966**, *11*, 895−904.
(80) Calvert, J. G.; Lazrus, A.; Kok, G. L.; Heikes, B. G.; Walega, J. G.; Lind, J.; Cantrell, C. A. Chemical Mechanisms of Acid Generation in the Troposphere. *Nature* **1985**, *317*, 27−35.
(81) Bhattacharya, S.; Agarwal, A. K.; Chanda, N.; Pandey, A.; Sen, A. K. *Environmental, Chemical and Medical Sensors*; Springer, 2017.
(82) Mustafa, A. K.; Gadalla, M. M.; Snyder, S. H. Signaling by Gasotransmitters. *Sci. Signaling* **2009**, *2*, re2.
(83) Szabo, C. Gasotransmitters in Cancer: From Pathophysiology to Experimental Therapy. *Nat. Rev. Drug Discov.* **2016**, *15*, 185−203.
(84) Bohrer, F. I.; Sharoni, A.; Colesniuc, C.; Park, J.; Schuller, I. K.; Kummel, A. C.; Trogler, W. C. Gas Sensing Mechanism in Chemiresistive Cobalt and Metal-Free Phthalocyanine Thin Films. *J. Am. Chem. Soc.* **2007**, *129*, 5640−5646.
(85) Tan, T. C.; Li, F.; Neoh, K. G. Measurement of BOD by Initial Rate of Response of a Microbial Sensor. *Sens. Actuators B Chem.* **1993**, *10*, 137−142.
(86) Jeon, J.; Lee, H.; Bao, Z. Flexible Wireless Temperature Sensors Based on Ni Microparticle-Filled Binary Polymer Composites. *Adv. Mater.* **2013**, *25*, 850−855.
(87) Uzunova, E. L. Theoretical Study of Nitrogen Dioxide and Nitric Oxide Co-Adsorption and $DeNO_x$ Reaction on Cu-SAPO−34 and Cu-SSZ−13 in Presence of Brønsted Acid Sites. *Mol. Catal.* **2018**, *447*, 47−55.
(88) Martínez-Ahumada, E.; López-Olvera, A.; Jancik, V.; Sánchez-Bautista, J. E.; González-Zamora, E.; Martis, V.; Williams, D. R.; Ibarra, I. A. MOF Materials for the Capture of Highly Toxic $H_2S$ and $SO_2$. *Organometallics* **2020**, *39*, 883−915.
(89) Nguyen, H. L.; Hanikel, N.; Lyle, S. J.; Zhu, C.; Davide Proserpio, D. M.; Yaghi, O. M. A Porous Covalent Organic Framework with Voided Square Grid Topology for Atmospheric Water Harvesting. *J. Am. Chem. Soc.* **2020**, *142*, 2218−2221.
(90) Morse, J. W.; Millero, F. J.; Cornwell, J. C.; Rickard, D. The Chemistry of the Hydrogen Sulfide and Iron Sulfide Systems in Natural Waters. *Earth Sci. Rev.* **1987**, *24*, 1−42.
(91) Lewis, R. S.; Deen, W. M. Kinetics of the Reaction of Nitric Oxide with Oxygen in Aqueous Solutions. *Chem. Res. Toxicol.* **1994**, *7*, 568−574.
(92) Mahajan, V.; Misra, M.; Zhong, K.; Fuerstenau, M. C. Enhanced Leaching of Copper from Chalcopyrite in Hydrogen Peroxide−Glycol System. *Miner. Eng.* **2007**, *20*, 670−674.
(93) Miracle, G. S.; Randall, S. L.; Liu, Z.; Brogden, D. W.; Ketcha, M. M.; Good, D. A.; Johnson, M. B.; Stenger, P. C.; Hertz, P. R.; Meli, F. Copper Chelants and Antioxidants in Laundry Detergent Formulations Reduce Formation of Malodor Moleculeson Fabrics. *J. Surfact. Deterg.* **2020**, *23*, 1125−1134.
(94) Glover, T. G.; Peterson, G. W.; Schindler, B. J.; Britt, D.; Yaghi, O. MOF-74 Building Unit Has a Direct Impact on Toxic Gas Adsorption. *Chem. Eng. Sci.* **2011**, *66*, 163−170.
(95) Zárate, J. A.; Sánchez-González, E.; Jurado-Vázquez, T.; Gutiérrez-Alejandre, A.; González-Zamora, E.; Castillo, I.; Maurin, G.; Ibarra, I. A. Outstanding Reversible $H_2S$ Capture by an Al (III)-Based MOF. *Chem. Commun.* **2019**, *55*, 3049−3052.
(96) Bhoria, N.; Basina, G.; Pokhrel, J.; Reddy, K. S. K.; Anastasiou, S.; Balasubramanian, V. V.; Al Wahedi, Y. F.; Karanikolos, G. N. Functionalization Effects on HKUST-1 and HKUST-1/Graphene Oxide Hybrid Adsorbents for Hydrogen Sulfide Removal. *J. Hazard. Mater.* **2020**, *394*, No. 122565.
(97) Rout, K. C.; Mondal, B. Aromatic C-Nitrosation by a Copper (II)-Nitrosyl Complex. *Dalton Trans.* **2015**, *44*, 1829−1835.
(98) Zhang, R.; Teoh, W. Y.; Amal, R.; Chen, B.; Kaliaguine, S. Catalytic Reduction of NO by CO over $Cu/CexZr1-xO_2$ Prepared by Flame Synthesis. *J. Catal.* **2010**, *272*, 210−219.
(99) Yao, M.; Wang, P.; Gu, Y.; Koganezawa, T.; Ashitani, H.; Kubota, Y.; Wang, Z.; Fan, Z.; Otake, K.; Kitagawa, S. A Comparative Study of Honeycomb-like 2D $\pi$-Conjugated Metal−Organic Frame-

work Chemiresistors: Conductivity and Channels. *Dalton Trans.* **2021**, *50*, 13236−13245.
(100) Wu, A.; Wang, W.; Zhan, H.; Cao, L.; Ye, X.; Zheng, J.; Naresh Kumar, P. N.; Chiranjeevulu, K.; Deng, W. H.; Wang, G.; Yao, M.; Xu, G. Layer-by-Layer Assembled Dual-Ligand Conductive MOF Nano-Films with Modulated Chemiresistive Sensitivity and Selectivity. *Nano Res.* **2021**, *14*, 438−443.
(101) Feng, X.; Yi, J.; Luo, P. The Influence Of $NO/O_2$ On The $NO_x$ Storage Properties Over A Pt-Ba-Ce/$\gamma$-$Al_2O_3$ Catalyst. *Open Chem.* **2019**, *17*, 1459−1465.
(102) Liu, G.; Gao, P. A Review of $NO_x$ Storage/Reduction Catalysts: Mechanism, Materials and Degradation Studies. *Catal. Sci. Technol.* **2011**, *1*, 552−568.
(103) Brozek, C. K.; Miller, J. T.; Stoian, S. A.; Dincă, M. NO Disproportionation at a Mononuclear Site-Isolated $Fe^{2+}$ Center in $Fe^{2+}$-MOF-5. *J. Am. Chem. Soc.* **2015**, *137*, 7495−7501.
(104) Wright, A. M.; Sun, C.; Dincă, M. Thermal Cycling of a MOF-Based NO Disproportionation Catalyst. *J. Am. Chem. Soc.* **2021**, *143*, 681−686.
(105) Fantauzzi, M.; Elsener, B.; Atzei, D.; Rigoldi, A.; Rossi, A. Exploiting XPS for the Identification of Sulfides and Polysulfides. *RSC Adv.* **2015**, *5*, 75953−75963.
(106) Kundu, M.; Hasegawa, T.; Terabe, K.; Yamamoto, K.; Aono, M. Structural Studies of Copper Sulfide Films: Effect of Ambient Atmosphere. *Sci. Technol. Adv. Mater.* **2008**, *9*, No. 035011.
(107) Lefèvre, G.; Bessière, J.; Ehrhardt, J.; Walcarius, A. Immobilization of Iodide on Copper (I) Sulfide Minerals. *J. Environ. Radioact.* **2003**, *70*, 73−83.
(108) Laajalehto, K.; Kartio, I.; Nowak, P. XPS Study of Clean Metal Sulfide Surfaces. *Appl. Surf. Sci.* **1994**, *81*, 11−15.
(109) Narjis, A.; Outzourhit, A.; Aberkouks, A.; Hasnaoui, M. E.; Nkhaili, L. Spectroscopic Study and Thermoelectric Properties of a Mixed Phase Copper Sulfide Lamellas. *J. Alloys Compd.* **2018**, *762*, 46−48.
(110) Hennemann, J.; Kohl, C.; Smarsly, B. M.; Metelmann, H.; Rohnke, M.; Janek, J.; Reppin, D.; Meyer, B. K.; Russ, S.; Wagner, T. Copper Oxide Based $H_2S$ Dosimeters − Modeling of Percolation and Diffusion Processes. *Sens. Actuators B Chem.* **2015**, *217*, 41−50.
(111) Thongtem, T.; Phuruangrat, A.; Thongtem, S. Characterization of Copper Sulfide Nanostructured Spheres and Nanotubes Synthesized by Microwave-Assisted Solvothermal Method. *Mater. Lett.* **2010**, *64*, 136−139.
(112) Fantauzzi, M.; Atzei, D.; Elsener, B.; Lattanzi, P.; Rossi, A. XPS and XAES Analysis of Copper, Arsenic and Sulfur Chemical State in Enargites. *Surf. Interface Anal.* **2006**, *38*, 922−930.
(113) Velásquez, P.; Leinen, D.; Pascual, J.; Ramos-Barrado, J. R.; Cordova, R.; Gómez, H.; Schrebler, R. XPS, SEM, EDX and EIS Study of an Electrochemically Modified Electrode Surface of Natural Chalcocite ($Cu_2S$). *J. Electroanal. Chem.* **2001**, *510*, 20−28.
(114) Güneri, E.; Kariper, A. Optical Properties of Amorphous CuS Thin Films Deposited Chemically at Different pH Values. *J. Alloys Compd.* **2012**, *516*, 20−26.
(115) He, M.; Yuan, L.; Zhang, W.; Hu, X.; Huang, Y. Enhanced Cyclability for Sulfur Cathode Achieved by a Water-Soluble Binder. *J. Phys. Chem. C* **2011**, *115*, 15703−15709.
(116) Park, J.; Yu, S.; Sung, Y. Design of Structural and Functional Nanomaterials for Lithium-Sulfur Batteries. *Nano Today* **2018**, *18*, 35−64.
(117) Georgiadis, A. G.; Charisio, N.; Yentekakis, I. V.; Goula, M. A. Hydrogen Sulfide ($H_2S$) Removal via MOFs. *Materials* **2020**, *13*, 3640.
(118) Bailey, T. S.; Zakharov, L. N.; Pluth, M. D. Understanding Hydrogen Sulfide Storage: Probing Conditions for Sulfide Release from Hydrodisulfides. *J. Am. Chem. Soc.* **2014**, *136*, 10573−10576.
(119) Bezdek, M. J.; Luo, S. L.; Liu, R. Y.; He, Q.; Swager, T. M. Trace Hydrogen Sulfide Sensing Inspired by Polyoxometalate-Mediated Aerobic Oxidation. *ACS Cent. Sci.* **2021**, *7*, 1572−1580.
(120) Duan, Y.; Pirolli, L.; Teplyakov, A. V. Investigation of the $H_2S$ Poisoning Process for Sensing Composite Material Based on Carbon Nanotubes and Metal Oxides. *Sens. Actuators B Chem.* **2016**, *235*, 213−221.
(121) Peterson, G. W.; Britt, D. K.; Sun, D. T.; Mahle, J. J.; Browe, M.; Demasky, T.; Smith, S.; Jenkins, A.; Rossin, J. A. Multifunctional Purification and Sensing of Toxic Hydride Gases by CuBTC Metal−Organic Framework. *Ind. Eng. Chem. Res.* **2015**, *54*, 3626−3633.
(122) Britt, D.; Tranchemontagne, D.; Yaghi, O. M. Metal-Organic Frameworks with High Capacity and Selectivity for Harmful Gases. *Proc. Natl. Acad. Sci. U. S. A.* **2008**, *105*, 11623−11627.
(123) Lin, X.; Wu, M.; Zhang, L.; Wang, D. Superior Stretchable Conductors by Electroless Plating of Copper on Knitted Fabrics. *ACS Appl. Electron. Mater.* **2019**, *1*, 397−406.


https://doi.org/10.1021/jacs.2c05510
J. Am. Chem. Soc. 2022, 144, 23297−23312